NRC·CNRC

NRC Publications Archive
Archives des publications du CNRC

Flow measurement by light interference

Zobel, Th.

For the publisher's version, please access the DOI link below./ Pour consulter la version de l'éditeur, utilisez le lien DOI ci-dessous.

Publisher's version / Version de l'éditeur:

https://doi.org/10.4224/20331573

Technical Translation (National Research Council of Canada), 1947-06-10

NRC Publications Archive Record / Notice des Archives des publications du CNRC :
https://nrc-publications.canada.ca/eng/view/object/?id=48cc403e-b61b-4fba-ac31-1028156c84a4
https://publications-cnrc.canada.ca/fra/voir/objet/?id=48cc403e-b61b-4fba-ac31-1028156c84a4

Access and use of this website and the material on it are subject to the Terms and Conditions set forth at
https://nrc-publications.canada.ca/eng/copyright
READ THESE TERMS AND CONDITIONS CAREFULLY BEFORE USING THIS WEBSITE.

L'accès à ce site Web et l'utilisation de son contenu sont assujettis aux conditions présentées dans le site
https://publications-cnrc.canada.ca/fra/droits
LISEZ CES CONDITIONS ATTENTIVEMENT AVANT D'UTILISER CE SITE WEB.

Questions? Contact the NRC Publications Archive team at PublicationsArchive-ArchivesPublications@nrc-cnrc.gc.ca. If you wish to email the authors directly, please see the first page of the publication for their contact information.

Vous avez des questions? Nous pouvons vous aider. Pour communiquer directement avec un auteur, consultez la première page de la revue dans laquelle son article a été publié afin de trouver ses coordonnées. Si vous n'arrivez pas à les repérer, communiquez avec nous à PublicationsArchive-ArchivesPublications@nrc-cnrc.gc.ca.

National Research Council Canada | Conseil national de recherches Canada

Canada

Ref
Ser
Q21
N2t4
no. TT-20
BLDG

COPY NO. 45

NATIONAL RESEARCH COUNCIL OF CANADA
DIVISION OF MECHANICAL ENGINEERING

IRC PUB

TECHNICAL TRANSLATION NO. TT-20

FLOW MEASUREMENT BY LIGHT INTERFERENCE

(STROEMUNGSMESSUNG DURCH LICHTINTERFERENZ)

BY TH. ZOBEL

BUILDING RESEARCH
FEB 18 1954
NATIONAL RESEARCH COUNCIL

ANALYZED

OTTAWA

10 JUNE, 1947

THIS REPORT MAY NOT BE PUBLISHED IN WHOLE OR IN PART WITHOUT THE WRITTEN CONSENT OF THE NATIONAL RESEARCH COUNCIL.

NATIONAL RESEARCH LABORATORIES

Ottawa, Canada

TECHNICAL TRANSLATION

Division of Mechanical Engineering

Pages - 23
Fig. - 35

Tech. Trans. TT-20
Date - 10 June 1947
File - 12-R4-22

Title: Stroemungsmessung durch Lichtinterferenz

By: Th. Zobel, Brunswick

Reference: Hermann Goering Aeronautical Research Institute
1 February 1940
ZWB FB 1167

Subject: Flow Measurement by Light Interference

Submitted by: W.F. Campbell
Head,
Aerodynamics Laboratory

Translated by:
D.A. Sinclair

Approved by: J.H. Parkin
Director

ABSTRACT

An optical measuring technique for the high speed wind tunnel of the LFA is being developed for quantitative and qualitative flow studies. The object is to determine the density on test bodies in the air flow and in their neighborhood by interference measurement.

The results so far obtained in simple preliminary experiments show that it is possible, even with small Reynolds numbers, to ascertain the density field surrounding a flow body by optical means. Simple, analytical relationships give the connection between density, pressure, velocity and temperature.

In addition interference measurement furnishes valuable information about boundary layer relationships, such as the type (whether laminar or turbulent) and thickness, as well as distribution of temperature and velocity.

TABLE OF CONTENTS

I INTRODUCTION

The development of an optical measuring technique for tests in the high speed wind tunnel at the Hermann Goering Aeronautical Research Institute, Brunswick (fig. 1) is based on the fundamental idea that the introduction of any mechanical measuring instruments whatsoever into a high speed flow must be avoided if the aim is to get measurement data not affected by disturbances. The extremely high propagation speed of light further recommended it for use as a measuring agency, since in this way even the most rapid phenomena in a flow can be registered completely free from inertia.

The choice fell upon an interference procedure with spatial separation of the interference beams in accordance with the Mach-Zehnder principle for analysing the density field surrounding a body subjected to a flow, and also for ascertaining the distribution of pressure on the test object itself.

An optical schlieren method is coordinated with the measuring procedure so that the flow phenomena may be made visible at the same time.

II THE INTERFERENCE-SCHLIEREN APPARATUS AT THE HERMANN GOERING AERONAUTICAL RESEARCH INSTITUTE, BRUNSWICK

The physical principles of the interference procedure have already been described elsewhere [1] to [5]. The basic plan shown in Figure 2 will serve to clarify the optical measuring equipment described below.

The light from a source L reaches the screen B via two different paths of equal length. The two plane parallel glass plates P_1 and P_2 are coated by evaporation with a thin layer of metal making them semi-transparent. The plane mirrors S_1 and S_2 are fully reflective. The light reaching plate P_1 is thus divided into two equally bright parts, of which one is reflected and the other allowed to pass through the plate.

From plate P_1, both partial light beams reach plate P_2 via S_1 and S_2 and can then be brought into interference.

A prerequisite for bringing about the interference is a careful basic adjustment of the apparatus in which all plates and mirrors must be parallel and the two light paths exactly equal. The beams then interfere at infinity.

In order to bring them into interference on a predetermined plane an adjustment of the angles at P_1 and P_2 must be made so that the two partial beams merge at the image plane B (fig. 3). We then get a strip system in this plane, which, by suitable adjustment of the mirrors, can be altered at will as to direction and width of the strips.

If a test medium of different density from the surrounding air is placed in the path of one of the two partial beams, called the test beam, a distortion of the interference strips occurs. The size of the bulge in a strip is a direct measure of the density in the test medium.

The adjustment of the angles in the interference refractometer determines the direction of the strip displacement in the interference image (fig. 3). This direction is positive or negative, depending on whether the two interference strips intersect to the right or left of the screen's (B) centre plane. To illustrate, figure 4 shows the spatial density field around a burning candle with the interferometer adjusted at different angles.

By choosing the width of strip the sensitivity of the interference procedure can be varied as desired within wide limits. By choosing the position of the strips and the sign of the bulging, the procedure can be favourably adapted to the particular test case.

If we are dealing, as in the field of aerodynamics, with the study of bodies within a flow, then by choosing our width of strip we can ascertain the distribution of pressure on the test object at a great many measuring points without the necessity of having pressure holes on the object itself.

Moreover, the density field as ascertained by interference yields data concerning the potential flow near the test object as well as valuable conclusions about boundary layer phenomena.

The schlieren procedure (fig. 2) is used for a simultaneous qualitative observation of the flow phenomena. The light, of different wave lengths, is brought from a source L' via a semi-transparent plane parallel plate P' to the test beam of the interference system. It proceeds with this beam simultaneously and in the same direction through the test medium. Thereafter the schlieren beam is separated from the interference beam by the second semi-transparent plate, P'', and likewise reaches the screen B over the schlieren stop. The result is a schlieren image of the flow phenomena of the same scale as the interference image.

Figure 5 shows diagrammatically the light path of the interference-schlieren apparatus designed at the Hermann Goering Aeronautical Research Institute. The light L, from an ultra-high pressure mercury lamp (upper left) of highest possible intensity is reflected at a small mirror, 1., onto the concave mirror, 2. It proceeds from there as a parallel beam to the guide mirror, 3, and then traverses the four-plate system as shown in figure 2. After the two partial interference beams have come together again at plate P_2, the light path continues via guide mirrors, 4 and 5, to reach the concave mirror, 6. This mirror, which has a large focal length (f = 3.5m), produces via mirrors 7, 8 and 9 an image of the test object in the wind tunnel. Mirror 9 is semi-transparent so that the light beam reaching it is divided into two parts. The stronger part is used for the image to be photographed; the weaker part is conducted via mirror 10 to a ground glass plate for observation. A colour filter installed in the light path serves to extract the wave lengths λ_1 = 5770/90 A.U., which are especially suited to our purposes.

The change in the optical path of the test beam, caused by the refractive index of the windows in the wind tunnel and of the end plates of the model, is equalized by a compensator in the path of the second beam.

The light path of the schlieren system begins at the source L' (lower left) and proceeds via mirrors 11 and 12 to the concave mirror, 13. From there the parallel beam reaches the test beam of the interferometer via the semi-transparent plate, 14. Together with this beam it passes through the air flow via the windows in the wall of the tunnel and the end plates of the test model (cf. fig. 2).

Plate 15 again separates the schlieren beam and directs it via the guide mirror, 16, to the concave mirror, 17. This, in turn, forms an image of the test model in the plane of the image to be photographed as well as that of the ground-glass plate. It has the same focal length and the same object distance and hence the same scale as the interference picture. The path is over the schlieren stop via mirrors 18 and 19.

Thus the course of the experiment can be observed continuously through both optical systems on a screen contained in a sound-proof compartment, while independently of this the same succession of events can be photographed or filmed. A high frequency motion picture apparatus per-

mits the filming of exceptionally interesting and rapid phenomena at high picture frequencies, while the light sources can be controlled from the motion picture camera to give brief, strong overloading (and thus an increase in light intensity).

For special tests of short-lived occurrences a flash installation is also provided for as an additional light source. This installation permits single photographs with exposure times of 10^{-6} second (fig. 5). Looking at the left-hand side of the diagram we can see that by simply changing the positions of mirrors 1 and 11 the spark illumination can be introduced into the two previously described paths of the optical system. The optical arrangement shown in figure 5 was chosen so as to reduce the large path distances in the apparatus itself before photographic reproduction, and so that both photography and observation could be undertaken close to the test area.

All optical-mechanical components are housed in a large test carriage built in the form of a box-girder, which can be insulated from the outside by heat-absorbing materials so as to shield the testing apparatus from surrounding temperature disturbances.

All mirrors and plates are mounted in universal arrangement. Each therefore is capable of angular rotation about two axes at right angles to each other. When the apparatus has been adjusted most of the mountings are locked. The only components which remain movable while the apparatus is in operation are plates P_1 and P_2 of the interferometer, the compensator, and the two plane parallel plates, 14 and 15, of the schlieren system.

The adjusting mechanisms of the mirrors, as well as the optical components[1] themselves, must be extremely precise, since angular adjustments as small as a fraction of a second must be possible.

The adjustable mirror units are fitted with multiple worm gears for fine adjustment. The reduction ratio is 1:73,000,000. The mirrors can be worked by electrical remote control from the test compartment, by means of which the smallest possible angular adjustment is 1/10 second.

1. All optical components were obtained from the firm of Halle and Sons, (Halle Nachf.), Berlin-Steglitz. The excellent universal mountings for the mirrors of the interferometer were also manufactured by Halle & Sons in accordance with our specifications.

An electrical indication of angular adjustment is linked to each drive mechanism so that an exact picture of the adjustment of the measuring equipment is always obtainable at the control desk.

The test carriage itself rests vibrotechnically on suspended beams, i.e., it is connected to the outer mobile supporting scaffold by accurately calibrated restoring springs. In this way the test apparatus is protected from all nearby shocks, whether they come from the wind tunnel or the building (fig. 6).

III INTERFERENCE MEASUREMENTS

While at present the scaffolding is still being designed, the interference part of the testing equipment has been in operation for about half a year with a provisional carriage of the original size. The first experiments have already been completed pertaining to optical compensation and to the angle sensitivity of glass plates introduced into the test beam as boundaries for the wind tunnel and the model. Further, a small experimental wind tunnel has been built so that flow measurements by means of light interference could already be carried out.

The bulging of the interference strips as compared with the undisturbed strip field (without air flow), provides a direct measurement of the density, in accordance with the equation

$$\Delta_y = \frac{b \cdot L (n_\infty - 1)}{\lambda \cdot \rho_\infty} \Delta\rho;$$

where Δ_y (mm) = the strip bulge;
b (mm) = the distance between two undisturbed interference strips;
$n_\infty - 1$ = refractive index in the undistrubed medium = $0.000293 \times \frac{273}{T_\infty}$

$\rho_\infty \left[\frac{kg\ s^2}{m^4}\right]$ = air density in undisturbed condition;
λ (mm) = wave length of light employed (5790 A.U.);
L (mm) = length of light path within the medium of altered density.

The magnitude $\frac{\Delta y}{b}$ is independent of the scale of magnification and can be derived from each strip picture.

For an adiabatic change of condition the relationship between density and static pressure in the flow field is given by the equation

$$\frac{p_1}{p_2} = \left(\frac{\rho_1}{\rho_2}\right)^k$$

If the static pressure on the surface of the submerged body is to be ascertained, then p and ρ are pressure and density on the test object and p_∞ and ρ_∞ are the pressure and density in the undisturbed flow. Thus in the first approximation we have

$$\frac{p-p_\infty}{p_\infty} = k\,\frac{\rho-\rho_\infty}{\rho_\infty}$$

When the Mach number is greater than 0.5, then, with the exact formula for the adiabatic processes we get

$$\frac{p}{p_\infty} = \left(\frac{\rho}{\rho_\infty}\right)^k$$

For the usual pressure coefficient $\frac{\Delta p}{q}$ in measurements of pressure distribution we thus get the following expression (for M 0.5):

$$\frac{\Delta p}{q} = \frac{p-p_\infty}{q_\infty} = k\,\frac{p_\infty}{q_\infty}\,\Delta\rho$$

The value $\Delta\rho$, however, is known from the optical measurement. Hence

$$\frac{\Delta p}{q} = k\,\frac{p_\infty}{q_\infty}\cdot\frac{\lambda}{L(n_\infty-1)}\cdot\frac{\Delta y}{b}$$

Numerical Example

For evaluating a density field

Span L = 170 mm.

Strip width on photograph b = 2.7 mm.

Dynamic pressure in the test section q = 350 $kg.m^{-2}$

p = 9975 $kg.m^{-2}$ at a temperature of 18° C.

$$\frac{\Delta p}{q} = \left(\frac{1.4 \times 9975}{350}\right)\left(\frac{5790 \times 10^{-7} \times 291}{170 \times 0.000293 \times 273}\right)\left(\frac{\Delta y}{b}\right)$$

$$\frac{\Delta p}{q} = 0.495 \times \frac{\Delta y}{b} = 0.183 \times \Delta y$$

Thus when the width of the strip is given the bulge needs only to be multiplied by a constant factor in order to get the pressure coefficient.

From the result obtained for Δy we see that the technique must be extremely sensitive to the smallest density changes, since the strip displacement measured in the interference picture is directly proportional to the strip width as well as to the length L (on an airfoil L is the span). Its remarkable sensitivity results from the fact that the density change occurring at each point in the flow field is integrated over the entire extension in depth (L) of the test medium. Through the choice of these two magnitudes b and L the sensitivity of the measuring technique can be adapted within wide limits to the experimental conditions in any given instance.

In this connection it should be mentioned that the theory of potential flow treats the air as an incompressible medium up to a flow speed of 100 meters per second, i.e., it is assumed that the density remains constant within this range. The fact, however, that in reality a change of density accompanies every change of speed, is just the principle of measurement underlying the interference technique. The assumption that the density in the potential flow is constant for all plane sections in the flow field is an error of negligeable proportions. However, the integral value of these small magnitudes, calculated over the length L, results in sufficient displacement of the interference strips for measuring purposes.

In the early stages of development of this optical technique it was supposed that in any case a far-reaching improvement in the sensitivity of the method would have to be sought. The results so far obtained, however, already show that even on a small model (170 mm. span), and at normal flow speed, satisfactory strip displacements are obtained. As a consequence the nature of the problem has changed fundamentally.

One has only to consider that the size of the strip bulge is proportional not only to b and L, but also to the change in density $\Delta\rho$ and consequently also to the square of the speed, or, in a compressible flow, approximately to the speed itself, to realize that large strip displacements must occur when tests are made in the high speed tunnel. If the span width, as used in these preliminary experiments, is multiplied by 10 and the speed of flow by 4, then with the strip width that has been thus far employed we can expect a strip displacement about forty times as great. It will therefore be necessary at times, when using the greatest possible speed of flow in the high speed wind tunnel, to reduce both the span width of the model and the width of strip in the interference picture considerably. No disadvantage results, aerodynamically, from using end plates at the extremities of the model (two-dimensional problem). The choice of the very narrow interference strips only increases the number of measuring points on the test object. For evaluation purposes, therefore, we can select at will whatever measuring points are considered important.

Figure 7 shows the density field of a cylinder of length L = 170 mm. and diameter D = 25 mm., at a flow velocity of 75 metres per sec., and with both signs of the strip displacement as determined by the adjustment of the angles in the interferometer. It is very clear, in the example given, that the direction of the strip bulges as shown in Figure 7a is the better for evaluation purposes, since there are a great many more measuring points to be had near the stagnation point and in the acceleration region. Note the pronounced transition in the densities from potential flow to the stagnation region, as well as the uniform intermediate value of the density behind the resistance body. Also to be noted is the way in which a very intense transfer of energy takes place in the two vortex trains at a distance of about one cylinder diameter behind the test body. This is caused by rapid changes in velocity. The haziness in the interference picture results from the fact that the frequency of the density changes is greater than that corresponding to the exposure time used, viz. 1/200 second. In the continuous picture of a slow motion camera we would see how rapidly the density variations occur.

Figure 8 shows the density distribution on the cylinder over a range of angles from 0° to 180°, as plotted from the interference measurement. For purposes of comparison a density distribution curve from R. and M. 1210 is placed alongside. The comparison shows that the optical measuring technique is reliable and supplies absolute values even under the primitive conditions of the small experimental

tunnel. This tunnel has as yet no honeycomb and the velocity distribution in the test section is very poor. Apparently, too, it has a very high turbulence level.

Figures 9 and 10 show the density field around an elliptic cylinder with an axis ratio of 4:1 at two different angles of attack, 0° and 8° and with both signs of the strip displacement. Figures 11 and 12 show the results of the interference measurement using both angles of attack and for comparison the result of the pressure distribution as calculated for zero incidence.

It is worth noting that the density distribution on the elliptic cylinder depends to a large extent on the Reynolds' number and on the turbulence level of the wind tunnel, as the results of the measurements in NACA Report No. 652 show. The curve of density distribution from the interference measurement is very similar to the result announced in the NACA Report for a different axis ratio. Complete agreement of the absolute values with the measurements from other tunnels and with the theory is not to be expected for the reasons mentioned.

In addition preliminary experiments on airfoil profiles were made. Figure 13 shows a series of attack angles of the profile Goe. 387, from which density distribution figures are derived. Since the profile in question has a thickness, amounting to 10 per cent of the tunnel diameter, the angular setting results in considerable changes in the flow field due to crowding of the jet. Calculations and comparisons can only be made, therefore, for $\alpha = 0°$ and, in some cases, $\alpha = 5.7°$. With other angles of attack the velocity in the test section can no longer be determined. For study purposes the photographs are given with the sign of bulge displacement that is the least favourable for evaluation. Note the distortion of the strips around the leading edge near the stagnation point.

Figure 14 shows the result of interference measurement on the profile Goe. 387 compared to the Goettingen pressure distribution measurement for $\alpha = 0°$. The deviation in the pressure distribution on the pressure side of the profile is caused by the disturbances due to the support.

Figures 15 and 16 show for the angle of attack $\alpha = 5.7°$ the influence of the support as this is placed respectively on the suction side and on the pressure side of the airfoil. Figure 17 gives the pressure distribution on the undisturbed profile (without support) as compared to the Goettingen pressure distribution curve.

In this experiment the disturbance due to the support is very noticeable, because in the first place the latter is placed very close to the wall of the tunnel, and secondly the span of the model is very small. In the high speed tunnel the relationships are much more favourable. Moreover it would be no problem to install the model in such a way that the supports would be outside the end plates and thus eliminate any influence of the disturbance on the flow against the airfoil itself.

Figures 18 and 19 show a series of angles of attack with a Joukowski profile of 10 mm. chord up to flow separation.

In all the interference pictures it can be seen that the strips in the stagnation region directly behind a resistance body, as well as those in the flow beyond at some distance from the model, show measurable bulgings from which the resistance can be ascertained. The evaluation procedure[1] for determining the resistance is now being worked out.

Up to this point it has been tacitly assumed that the interference strips are produced by monochromatic light with the entire image field made up of saturated interference strips. Homogeneous light was indeed used in all the examples so far shown. There are, however, instances of application where it is necessary to identify single strips. For this reason certain ones must be accentuated. This occurs in the so-called zero-interference, where single strips of different degrees of saturation and distinctness appear.

If we use a light that emits several wave lengths these will give different interference strip widths. The result is a group formation of strips. Between the individual strip groups, at the place where the maximum intensity of one colour system coincides exactly with the minimum intensity of another, the light is wholly extinguished and no interference takes place. There is only one strip group containing a heavily saturated strip, the so-called zero-interference, which is formed in the line of symmetry of all coherent points of light. The presence of this zero-interference is at the same time the criterion for complete adjustment of the interferometer. At this stage the two light paths (fig. 2 and 3) must be so nearly equal in length that they differ only by fractions of half a wave length of the light employed.

1. A separate report is being issued on the evaluation procedure in interference measurement.

Figure 20 shows a picture of zero-interference from a mercury vapour lamp. The zero-interference strip is clearly distinguishable from the others by its heavy blackening.

Figure 20 shows further, how advantageously the zero-interference can be used to ascertain, for example, the velocity in the closed wind tunnel. If the upper part of the photograph represents the interference strip picture with the known original condition of the wind tunnel without flow ($v = 0$), then the lower part shows the displaced strip field under flow. The extent of the displacement is directly proportional to the change in density and therefore to the flow velocity. Similarly temperature and fluidity strata and the like, can be measured with zero-interference, since these characteristics of the otherwise homogeneous test medium are accompanied by density variations.

IV BOUNDARY LAYER INVESTIGATIONS

The interference pictures of the airfoils subjected to flow already show other very interesting results which also lend themselves to the measurement of pressure distribution. The formation of the boundary layer and its increasing thickness in the direction of the chord is clearly recognizable on the surface of the profile. In the examples so far studied we have been dealing exclusively with a turbulent boundary layer which may be as much as several millimetres thick on the edge of the airfoil.

The law of potential flow holds good only outside the boundary layer. Therefore the measuring points for the evaluation lie on the boundary line of potential flow, from which the interference strips proceed at a sharp angle to the profile surface. At places where there is no boundary layer the measuring points lie on the surface of the profile.

Since Bernouilli's equation is not valid within the boundary layer--on the contrary the static pressure through its thickness, in a direction perpendicular to the surface, can be taken as constant--it follows that the strip displacement in the interference picture comes solely from a temperature effect in the friction layer. Strip displacement is most pronounced at the point of greatest heating, that is, at that point on the airfoil surface where the velocity has the value zero. The temperature distribution in the boundary layer itself can therefore be determined from the general equation of state $\frac{p}{\rho} = R.T$, since the static pressure at the edge of the boundary layer, is known from the pressure in the potential flow.

The question, whether the assumption of constant pressure within the boundary layer is justified, can be answered with the help of the interference pictures. If a change of pressure took place within the boundary layer, it would have to be indicated in the displacement of strips. The extension of each strip in the potential flow to the surface of the profile would have to lead to points which showed a lateral displacement in relation to the points at the edge of the boundary layer. This amount would then correspond to the change of static pressure in the boundary layer. From all the interference photographs, however, it is very clear that at the place where the boundary layer is thick the strips run almost vertical, and at other places, where they are bent, the boundary layer is almost zero. In no case, however, do we discern a strip displacement which would be large enough to merit our notice.

There is so far no other method of measurement which makes the boundary layer visible and measurable as the interference method does. Figure 21 gives the thickness of the boundary layer on the Joukowski profile at the three angles of attack 0°, 4° and 8° (cf. fig. 18). For purposes of comparison the measured boundary layer thickness for 0° on a somewhat thicker symmetrical Joukowski profile is included, taken from R. and M. 1315. Figure 22 shows the boundary layer thickness on the elliptical cylinder for three different angles of attack (see also figures 9 and 10).

Another important example for studying the boundary layer is given by the flat plate at zero incidence. Although the pressure of the undisturbed flow prevails on its surface, there is nevertheless a pronounced change in density, which corresponds, therefore, to a simple temperature effect.

Figure 23 shows an enlarged section of the density field around the flat plate and the density effect in the boundary layer. Two different strip widths are used and the Reynolds' number is Re = 800,000.

Exact experiments on boundary layer phenomena in which there is a transition from laminar to turbulent boundary layer can be carried out only under the aerodynamically satisfactory conditions of the high speed wind tunnel with the turbulence level known. The large span of the model then provides a means of making the laminar boundary layer visible even at low speeds.

V ANALYTICAL RELATIONSHIP BETWEEN DENSITY, PRESSURE, VELOCITY AND TEMPERATURE.

Notation:

p = pressure
ρ = density
T = absolute temperature
v = velocity

} at a chosen point in the flow field.

$p_\infty, \rho_\infty, T_\infty, v_\infty$ = corresponding values in the undisturbed flow at considerable distance from the body.

p_s, ρ_s, T_s, v_s = corresponding values at the outer edge of the boundary layer.

$\Delta p = p - p_\infty$
$\Delta \rho_1 = \rho - \rho_\infty$ (in potential flow)
$\Delta \rho_2 = \rho_s - \rho$ (in boundary layer)
$k = \frac{c_p}{c_v} = 1.4$ for air
$M = (\frac{v}{a})$ = Mach number in the undisturbed flow
a = velocity of sound in the undisturbed flow.

By an analytical approach Prof. Schlichting[1] obtains the following simple equations concerning the relationship between density, pressure, velocity and temperature, based on the general equation of state and the law of conservation of energy:

1. For potential flow.

(a) For small Mach numbers

Relationship between pressure and density:

$$\frac{p - p_\infty}{p_\infty} = k \frac{\rho - \rho_\infty}{\rho_\infty}$$

Relationship between temperature and density:

$$\frac{T - T_\infty}{T_\infty} = (k - 1) \frac{\rho - \rho_\infty}{\rho_\infty}$$

---

1. A special report by Prof. Schlichting concerning the theoretical procedure is to appear.

Relationship between velocity and density:

$$\frac{v^2 - v_\infty^2}{v_\infty^2} = -\frac{2}{M^2}\frac{\rho - \rho_\infty}{\rho_\infty}$$

(b) For large Mach numbers

Relationship between pressure and density:

$$\frac{p}{p_\infty} = \left(\frac{\rho}{\rho_\infty}\right)^k$$

Relationship between temperature and density:

$$\frac{T}{T_\infty} = \left(\frac{\rho}{\rho_\infty}\right)^{k-1}$$

Relationship between velocity and density:

$$\frac{v^2 - v_\infty^2}{v_\infty^2} = \frac{2}{(k-1)M_\infty^2}\left[1 - \left(\frac{\rho}{\rho_\infty}\right)^{k-1}\right]$$

For this series of calculations frictionless flow is assumed, in which no exchange of energy with the surrounding space takes place due to heat conduction, heat radiation or convection.

2. For the boundary layer

Relationship between pressure and density:

$$p - p_s = 0$$

Relationship between temperature and density:

$$\frac{T - T_s}{T_s} = \frac{\rho_s - \rho}{\rho} = \frac{-\frac{\rho - \rho_s}{s}}{1 + \frac{\rho - \rho_s}{\rho_s}}$$

Relationship between velocity and density:

$$\frac{v^2 - v_s^2}{v_s^2} = \left(\frac{-2}{(k-1)M_s^2}\right)\frac{\rho_s - \rho}{\rho} = \frac{2}{(k-1)M_s^2}\left(\frac{\frac{\rho - \rho_s}{\rho_s}}{1 + \frac{\rho - \rho_s}{\rho_s}}\right)$$

In contrast to the analytical assumption for potential flow, the law of conservation of mechanical energy (Bernouilli's equation) has simply been substituted here following the hypothesis, usual in connection with the boundary layer theory, that the pressure within the boundary layer is constant at right angles to the surface subjected to flow.

Since the equation for the relationship between density and temperature in the boundary layer neglects a transfer of heat, the temperature distribution obtained by calculation must result in values that are too large.

An evaluation of the interference pictures has been made for the example of the flat plate (fig. 23).

Figure 24 shows the velocity distribution in the boundary layer of the flat plate as calculated for turbulent boundary layer by the law of 1/7 powers. For comparison the results of the interference measurement are also shown.

Figure 25 gives the calculated temperature distribution in the boundary layer of the flat plate as well as the interference measurement. We note that the latter, corresponding directly to the actual density gives smaller temperature values than the calculation. This result was to be expected, as the calculation ignores any decrease in the temperature in the boundary layer due to conduction or radiation of heat or to convection. To discover whether the difference in the results corresponds exactly to the absolute amount of temperature decrease through heat transfer, requires testing by careful studies in the high speed wind tunnel.

VI FURTHER POSSIBLE APPLICATIONS OF THE INTERFERENCE TECHNIQUE

The fact that measurement with the aid of light is completely free from inertia and is therefore suitable even for occurrences of movement which happen very swiftly, opens up entirely new possibilities, the limits of which cannot yet be foreseen, for applying the interference technique. Of special interest in this connection are those non-steady phenomena on airfoils in which, at times, the motion is so rapid that the flow process cannot keep up with it. The simplest example of this kind is the transient increase of lift on the airfoil accompanying a sudden increase in the angle of attack.

Measurements which, taken together, indicate an increase in the maximum lift (squall effect), are not enough to explain this effect. Nor do they give any clue as to the behaviour of lift when the angle of attack is suddenly altered in the region of small c_a values; nor as to the displacement of the centre of lift; nor to the part played by the boundary layer in non-steady flow processes.

Another very important series of questions is raised by the oscillating airfoil itself, as well as the foil with fixed, extended flap and loose rudder.

Until now there has been no method which permits measurement of the density distribution on the oscillating wing simultaneously at many test points while it is in motion, and which, in addition, gives information about the boundary layer phenomena.

It is difficult enough to dispose a large number of testing points on a small airfoil model for tests of steady phenomena at high speed, while leading the bundles of connecting tubes out of the air stream to the pressure recording instrument with as little disturbance to the flow process as possible. But it is much more difficult to lead off non-steady pressure measurements from the oscillating airfoil.

The investigation of such questions presents no problem for the interference method, since each instantaneous picture gives the complete distribution of density on the profile and in its neighborhood, as well as in the boundary layer.

Experiments made to date with an airfoil undergoing torsional vibration at the rate of forty oscillations per sec. are recorded on slow motion films and show the density field changing with each movement. Each single interference picture contains all the measurement data required for analysing and evaluating the flow process. It thus becomes possible to ascertain the relationships on the oscillating airfoil in connection with the problem of rudder compensation, and also to determine the propagation of pressure waves on the profile surface at high speeds with the resulting change in lift and displacement of the centre of pressure.

Figure 27 shows a strip of pictures from a miniature slow motion film (original size shown in figure 27a) of the Joukowski airfoil subjected to a flow velocity of 75 metres per sec. and oscillating at 40 c.p.s.

Interference measurements should also prove very useful in investigating radiator shapes for high flying speeds. It is well known that the resistance relationships of spindle-body nozzle radiators (Spindelrumpfduesenkuehlern) become very favourable when the cooling stream flows out of the fuselage at a point of available excess speed and then falls upon the rest of the flow body. Up to the present we can only guess at the causes of these phenomena arising with unheated radiators. Even pressure distribtion measurements, which could be carried out at many measuring points only by much selection, do not clarify these problems satisfactorily if the boundary layer ratios are left out of account.

When a flat radiator model is used the interference measurement gives all the density ratios, i.e., pressure and velocity on the outer body as well as at every point of the intake channel and of the diffuser, and in addition gives information about the boundary layer and its influence throughout the wind stream. The development of a suitable nose shape at the intake point of the radiator for various flow passages and angles of attack is likewise furthered by interference measurement. If one knows the ratios in the case of the plane problem, it is then possible to carry over the results to rotationally symmetrical examples.

If the results of the plane problem are carried over to the denisty field of a rotationally symmetrical body as developed in one plane, we seem to come nearer (at zero incidence in any case!) to the actual ratios than with a flow test of the three-dimensional density field. Owing to the fact that the light rays in the three-dimensional density field must traverse different zones of varied and unknown densities, some uncertainty is always present in the evaluation of the separate phenomena. The exploration of three-dimensional density fields is an important task for the immediate future.

For plane problems the representation has the great advantage of permitting no ambiguity to arise as to processes and evaluation, while for the analysis of the three-dimensional density field at the present stage of development one must still be content with a very awkward graphical interpolation procedure as a method of approximation. An additional great advantage of the plane problem is that the interference measurement also allows us a glimpse of what occurs in the interior of a body, for example in the diffuser, and in the flow passages of radiators, and in the slots behind spoiler flaps on models and the like. Thus there are a number of further possibilities of applying the interference procedure in problems which are outside the scope of the earlier measuring technique.

Figures 28 to 31 show as an example a plane model of a NACA radiator cowling subjected to a flow velocity of 75 metres per second. Two different designs are shown: one with a somewhat extended, very rounded hub, and the other with an ordinary (NACA), short hub only slightly rounded. In figures 28 and 30 the flow passage is open; in figures 29 and 31 it is plugged. Figure a gives the undisturbed interference strip field in each case for no air flow; figures b, c and d give the flow relationships at three different angles of attack, 0°, 4° and 8°.

Even before analysis the interference strip pictures lead to conclusions about the flow process on and within the radiator cowling and about the relative suitability of the respective shapes. From the interference strip pictures we are able, by means of the simple analysis indicated on pages 5 and 6, to deduce the prevailing velocity at every point on the hub and in the flow channel.

Here, however, we might just point out some differences in connection with the evaluation of the radiator shapes which can be discerned even with the eye. From the sharp deviations of the interference strips near the noses and from the way in which they change as the angle of attack is altered we recognize the presence of excess velocity in this region. With the closed form in figure 29, hub and cowling operate as a single shape to which the flow adheres. It can be seen clearly that a region of still air forms in the closed flow passage around which the external flow streams as if over a profile contour.

Figures 28b, c and d show that the excess speed on the projecting hub is considerably greater than with the closed shape. From this we realize that when there is a flow through the passage the two noses, of hub and cowling, form separate flow profiles. The velocity in the flow passage appears to be at its greatest when $\alpha = 4°$, whereas with $\alpha = 8°$ a screening effect has already come into operation on the suction side. At 8° the flow still adheres to the nose of the hub.

In figures 28b and c, a sharp change in density can be recognized behind the region of greatest excess speed on the suction side of the hub. This apparently represents the transition from laminar to turbulent boundary layer. The portion of the layer lying behind it, is unmistakably recongizable as turbulent boundary layer, merely from its considerable thickness. The point of transition from laminar to turbulent layer moves farther forward with large angles of attack. The smooth part of the cowling acts as a flat plate.

Figures 30 and 31 show that even on the slightly rounded nose the flow breaks away at an angle of attack of 0°. The difference between the increased velocity on the outer body and the zero velocity in the closed flow passage is clearly recognizable from the picture series 31b, c and d. The flow through the passage of the radiator with short hub exerts a considerably stronger and less favourable influence on the outer flow than is the case with the design illustrated in figure 28. Even at $\alpha = 4°$ we recognize a sharp increase in the thickness of the boundary layer and an approach to the critical state where the flow breaks away on the outer portion of the body. Figure 30d shows how, at $\alpha = 8°$, the flow on the suction side has already broken away from the outer portion of the cowling.

Presumably the favourable condition of attached flow could be attained merely by rounding the short hub more and pulling it just slightly forward. The screen effect hindering the flow through the passage at larger angles of attack then disappears. Whether the flow in the example of the last named design still adheres to the body when the angle of attack is relatively large has still to be investigated.

As an additional example, interference pictures of flow over a nozzle radiator with a large flow opening are shown in figures 32 to 35. In figures 32 and 33 a permeable resistance plate containing horizontal slits and having a transmission of 50 per cent has been fitted into the flow passage. Figure 32a shows (see also figure 7) how at a short distance behind the resistance plate the density has been equalized to an almost constant mean value over the entire cross section. (None of the interference strip fields has been retouched in any way!)

We can determine the velocity at different points in the flow passage directly from the displacement of the strips. The series of pictures in the right-hand columns (fig. 33 and 35) shows the arrangement with a hinged flap, in which a considerable increase of velocity in the flow passage can be recognized very plainly. Figures 34 and 35 show the interference strip picture as flow passes through the open nozzle passage without and with the hinged flap effect respectively.

These examples merely show how simply interference measurement permits such experiments at quite a small technical experimental expense (provided an interferometer is available) and affords a glimpse of many processes that are still unknown otherwise. The interference analysis furnishes the quantitative data for these processes.

The application of optical measuring techniques grows more and more urgent as flying speed increases, for they possess the great merit of allowing us to make processes visible and measurable without the processes themselves suffering any disturbance whatsoever. Another great advantage connected with interference measurement is that all pressure holes in the model are eliminated and the manufacture of the once very complicated and expensive models (e.g. models with pressure holes for high speed studies) is greatly simplified. Moreover, from the point of view of measuring technique, it is very useful to have every interference picture, even those made at high frequency on slow motion film, contain all the measurement data of the test process.

VII SUMMARY

A new optical measuring technique, developed in the Hermann Goering Aeronautical Research Institute at Brunswick, is described for simultaneous qualitative and quantitative representation of density fields surrounding bodies subjected to flow. It was worked out particularly for experiments under conditions of compressible flow in the high speed wind tunnel. However, the results so far obtained from preliminary trials with the interference part of the measuring equipment prove that even at ordinary velocities it is possible to get density fields that we can evalutate on bodies subjected to flow.

Simple analytical relationships give the connection between density, as obtained by interference of light, and pressure, velocity and temperature on the test body and in its neighborhood. The process of analysis for pressure distribution is explained and the usefulness of the method is proven in numerical examples. At the moment work is being done on the evaluation of resistance by interference.

It is further shown that the optical measuring technique makes it possible for the first time to visualize the boundary layer and to obtain its quantitative data. Owing to the high propagation speed of light all phenomena in the flow can be recorded by the optical method entirely without inertia, no matter how swiftly they take place. Because it is possible to investigate events that were utterly beyond the scope of the previous measuring technique, many more possibilities of application arise for the interference method in connection with a number of new problems. We cannot yet estimate the extent of these possibilities.

BIBLIOGRAPHY

1. E. Gehrcke, Die Anwendung der Interferenzen in der Spektroskopie und Metrologie (The Use of Interference in Spectroscopy and Metrology); Brunswick, 1906.

2. H. Schardin, Theorie und Anwendung des Mach-Zehnderschen Interferenzrefraktometers (Theory and Application of the Mach-Zehnder Interference Refractometer); Z. Instrumentenkde, Vol. 53 (1933), pp. 396, 424 and 430.

3. A. v. Dechend, Ueber die genaue Messung der Lichtbrechung in Gasen (On the Exact Measurement of Refraction of Light in Gases); Heidelberg, 1913.

4. Th. Zobel, Verwendung von Lichtinterferenzen in der technischen Messung (The Use of Light Interference in Technical Measurement); Z. VDI, Vol. 81 (1937), No. 18, p. 503.

5. Th. Zobel, Entwicklung und Bau eines Interferenzgeraetes zur optischen Messung von Dichtefeldern (Development and Construction of an Interferometer for Measuring Density Fields by Optical Means); FB 1008.

Fig. 1
Tech. Trans. TT-20

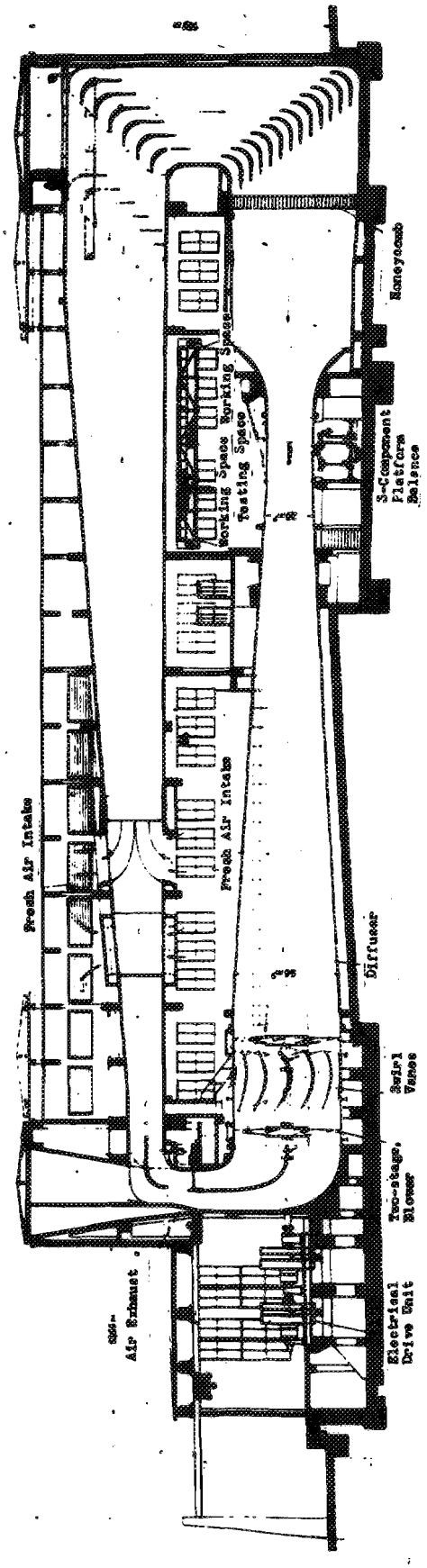

Fig. 1 High Speed Wind Tunnel, Hermann Woering Aeronautical Research Institute, Braunschweig.

FIG. 2&3
TECH. TRANS.
T. T.-20

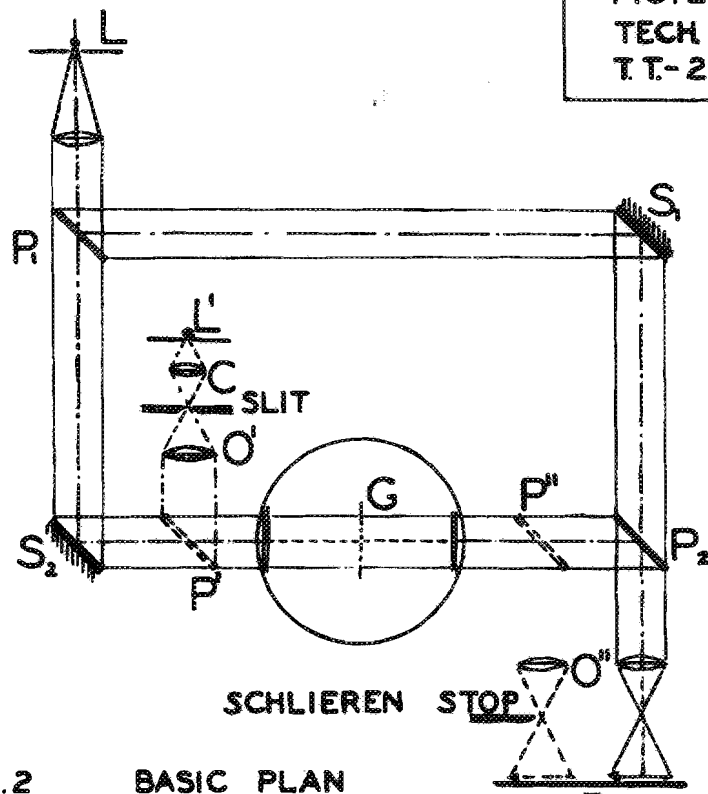

FIG. 2 BASIC PLAN OF THE LIGHT PATH IN THE INTERFEROMETER

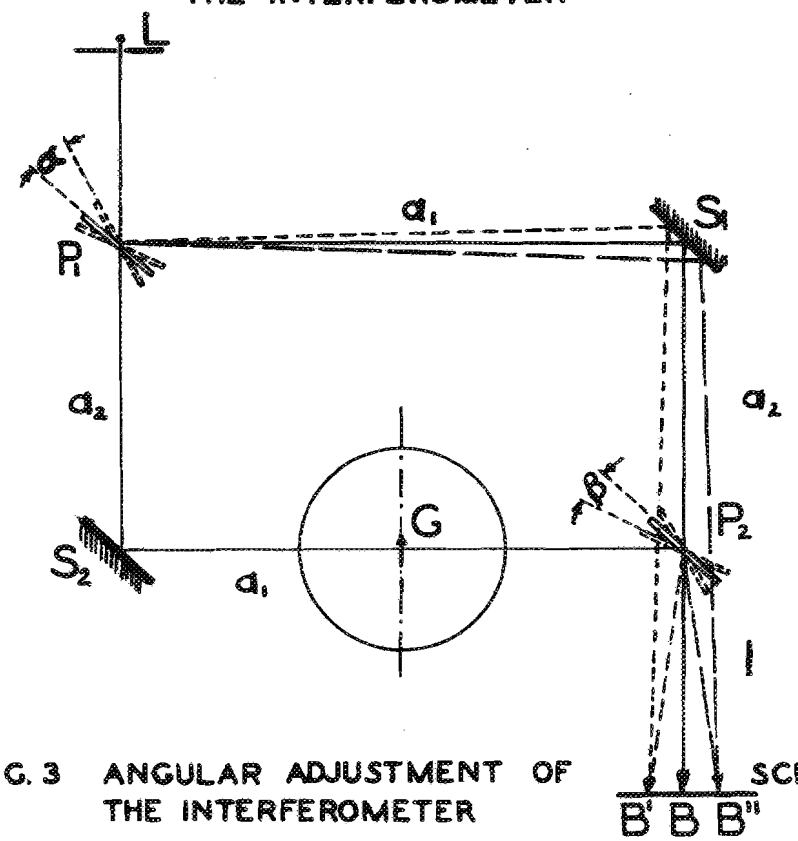

FIG. 3 ANGULAR ADJUSTMENT OF THE INTERFEROMETER

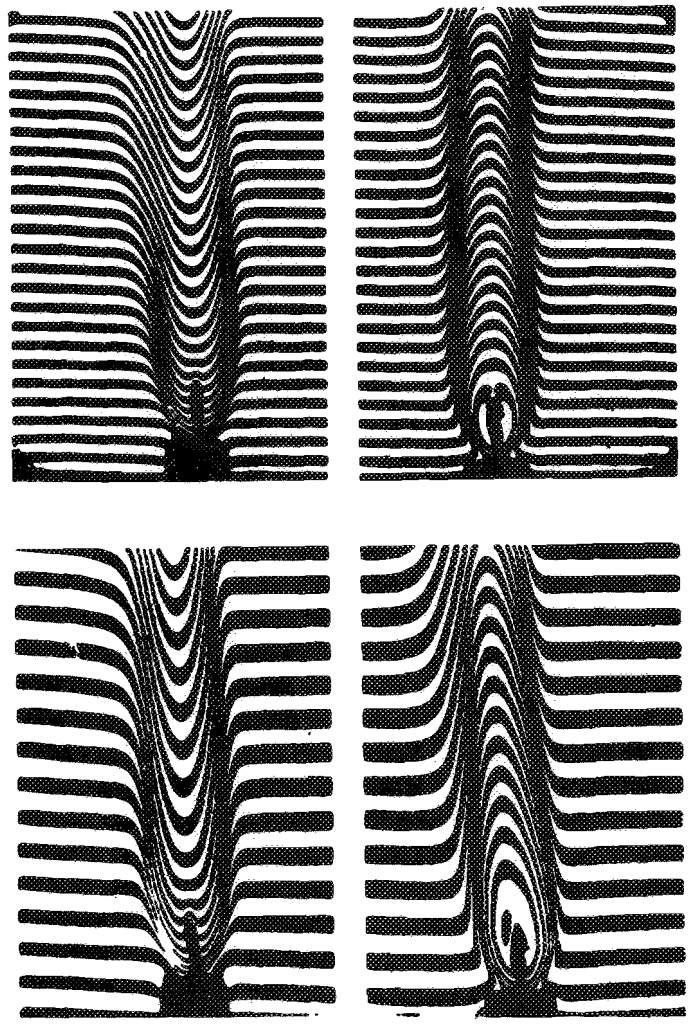

Fig. 4. Spatial Density Field Around a Flame Showing Strips Bulging in Both Directions

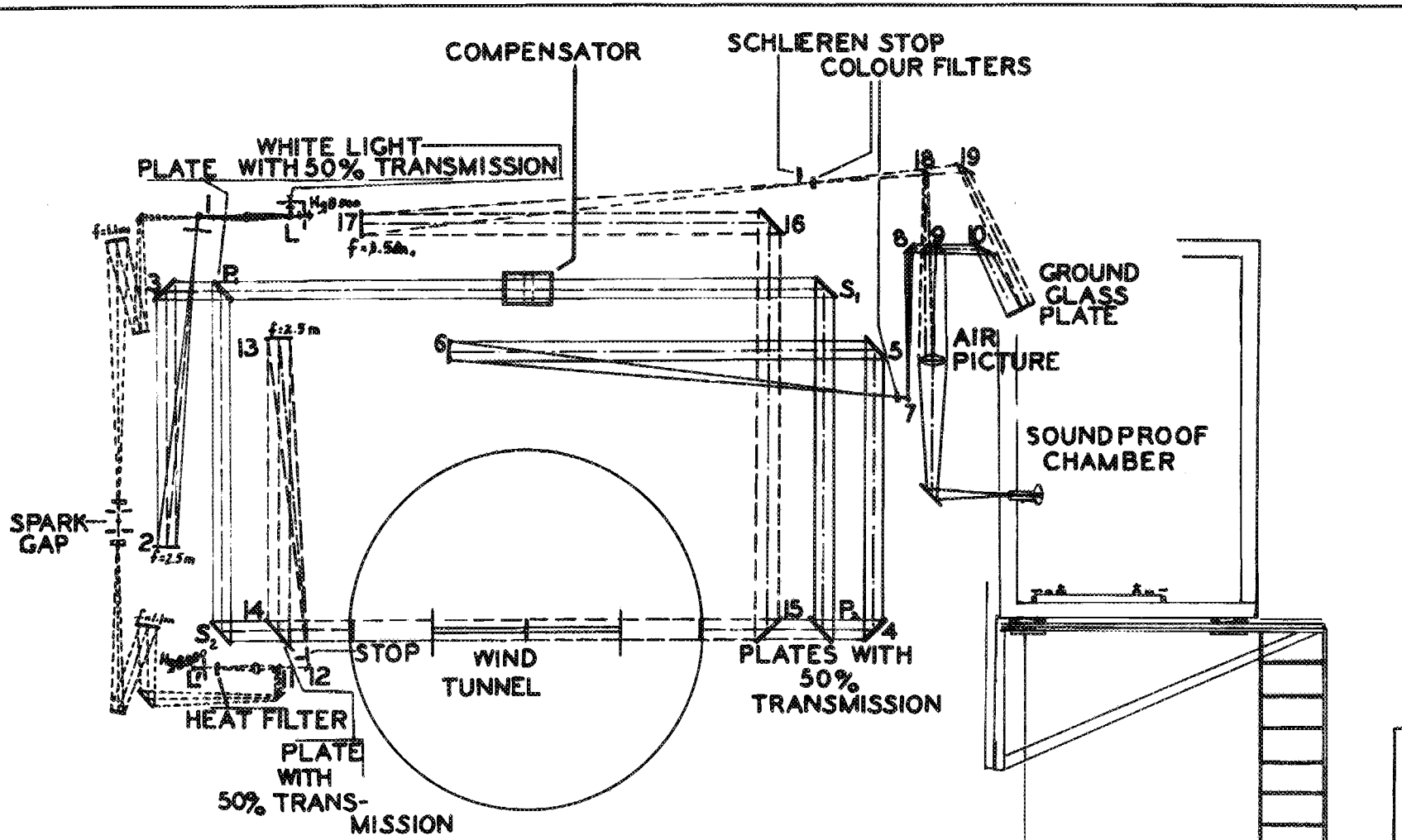

FIG. 5 INTERFERENCE-SCHLIEREN PROCEDURE

FIG. 5
TECH. TRANS.
T.T.-20

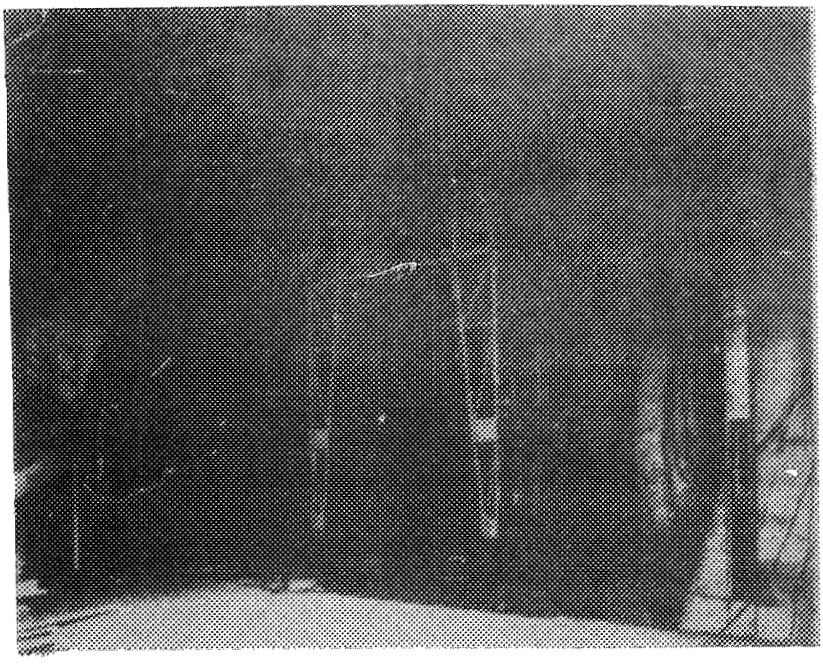

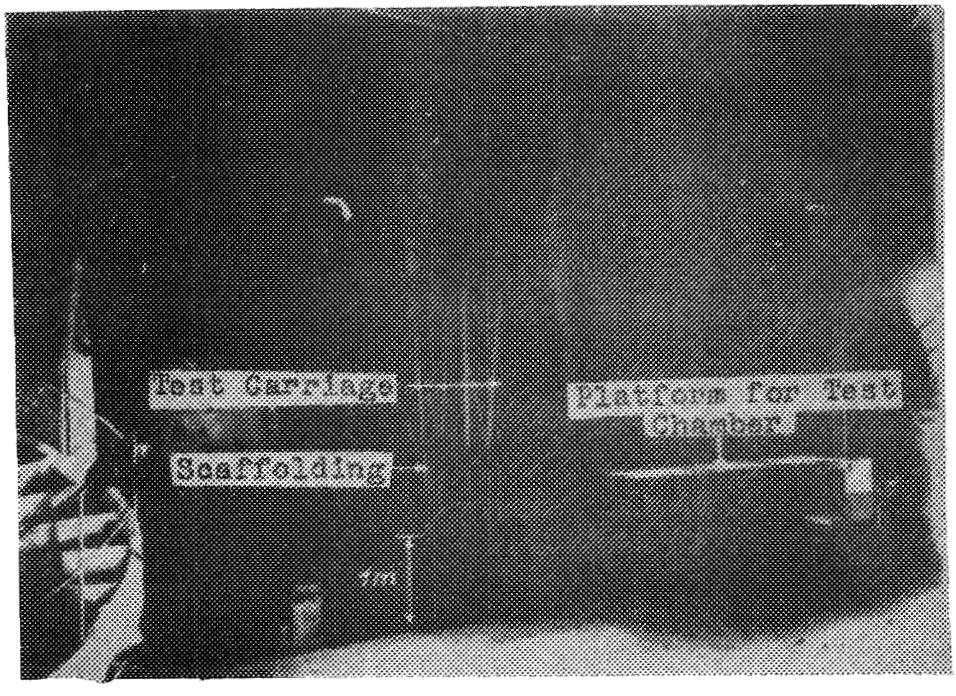

Fig. 6. Mobile Scaffolding of the LFA Interference-Schlieren Apparatus at the Test Section of the High Speed Wind Tunnel

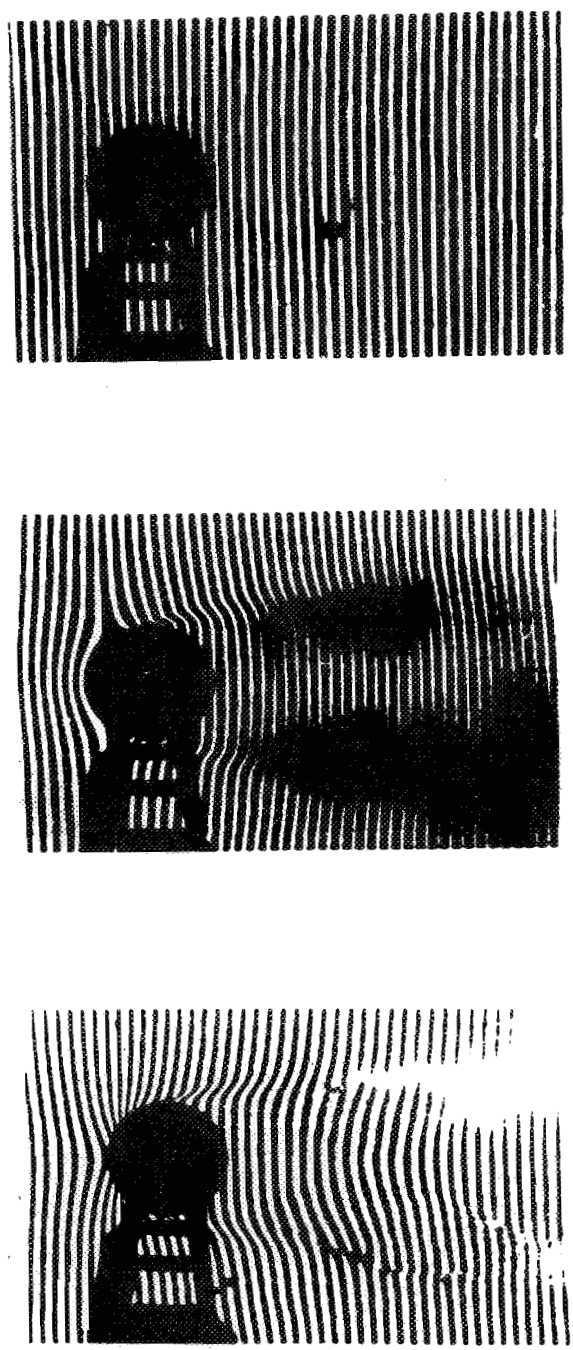

Fig. 7. Density Field on Circular Cylinder in Air Flow
Diameter=25 mm; v = 75 m/sec; L = 170 mm.

Fig. 8
Tech. Trans. TT-20

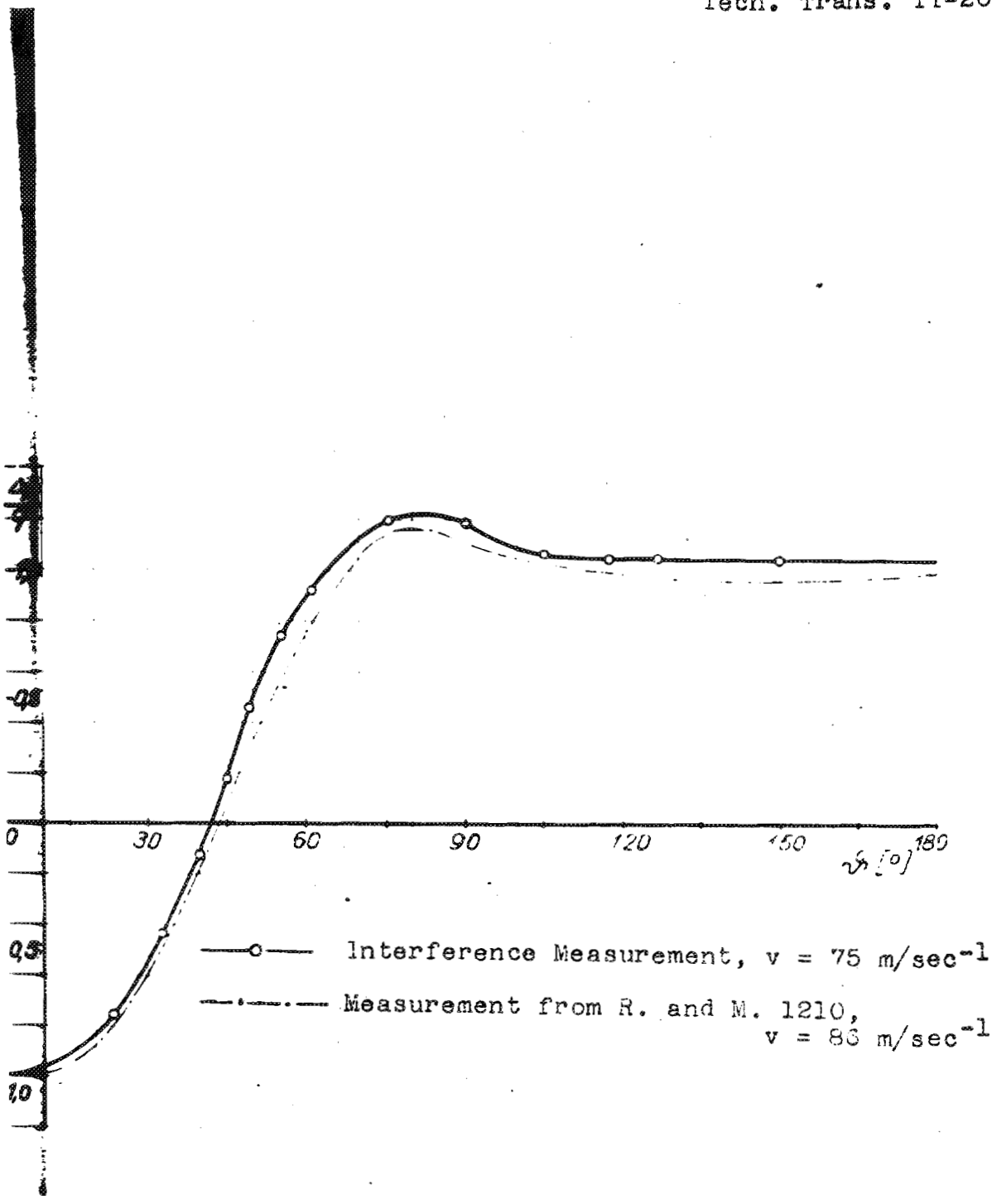

Fig. 8. Density Distribution on Circular Cylinder

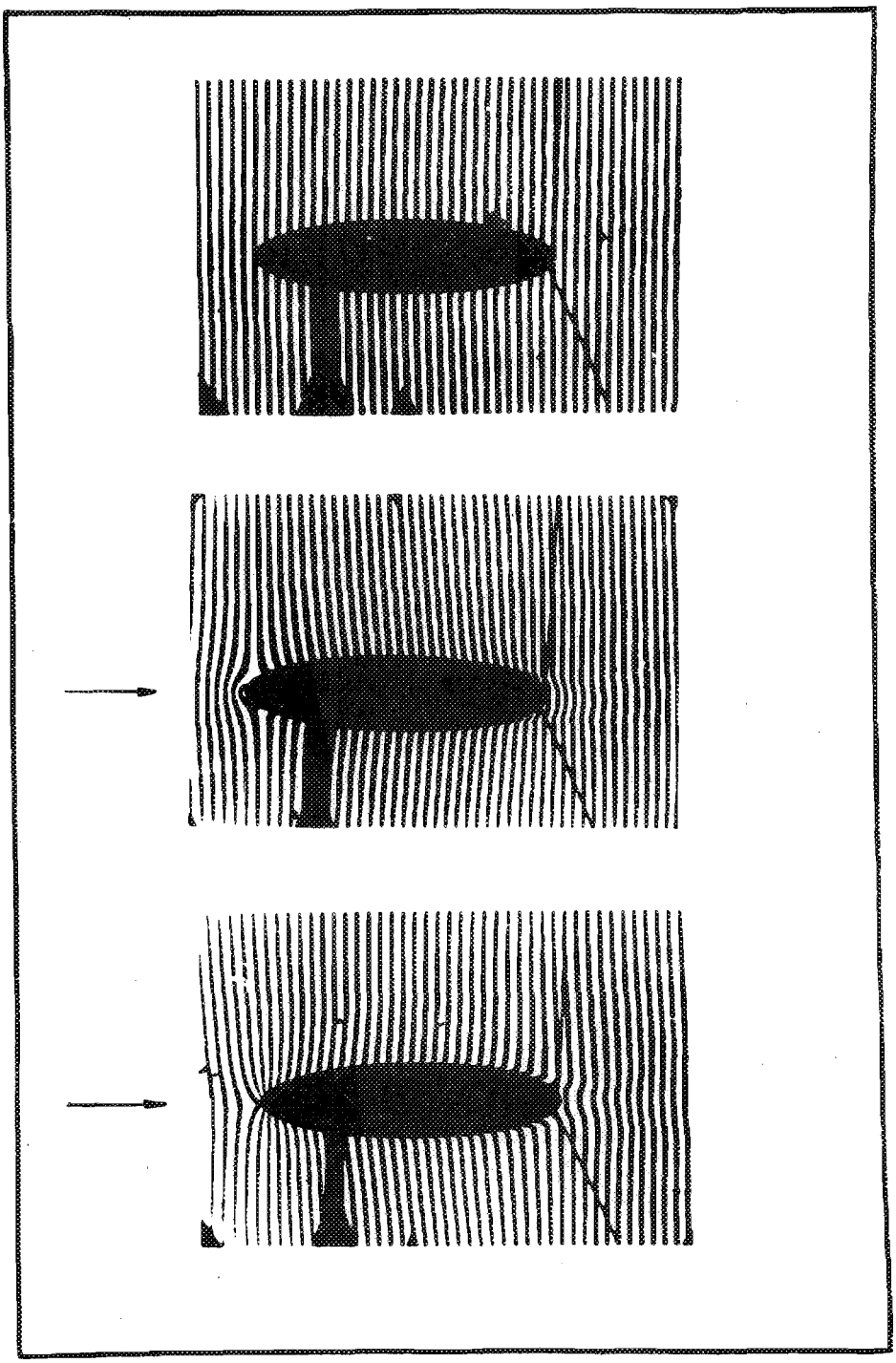

Fig. 9. Density Field on Elliptic Cylinder at $\alpha = 0^{\circ}$

$2a = 80$ mm; $\frac{b}{a} = \frac{1}{4}$; $L = 170$ mm; $v = 75$ m/sec.

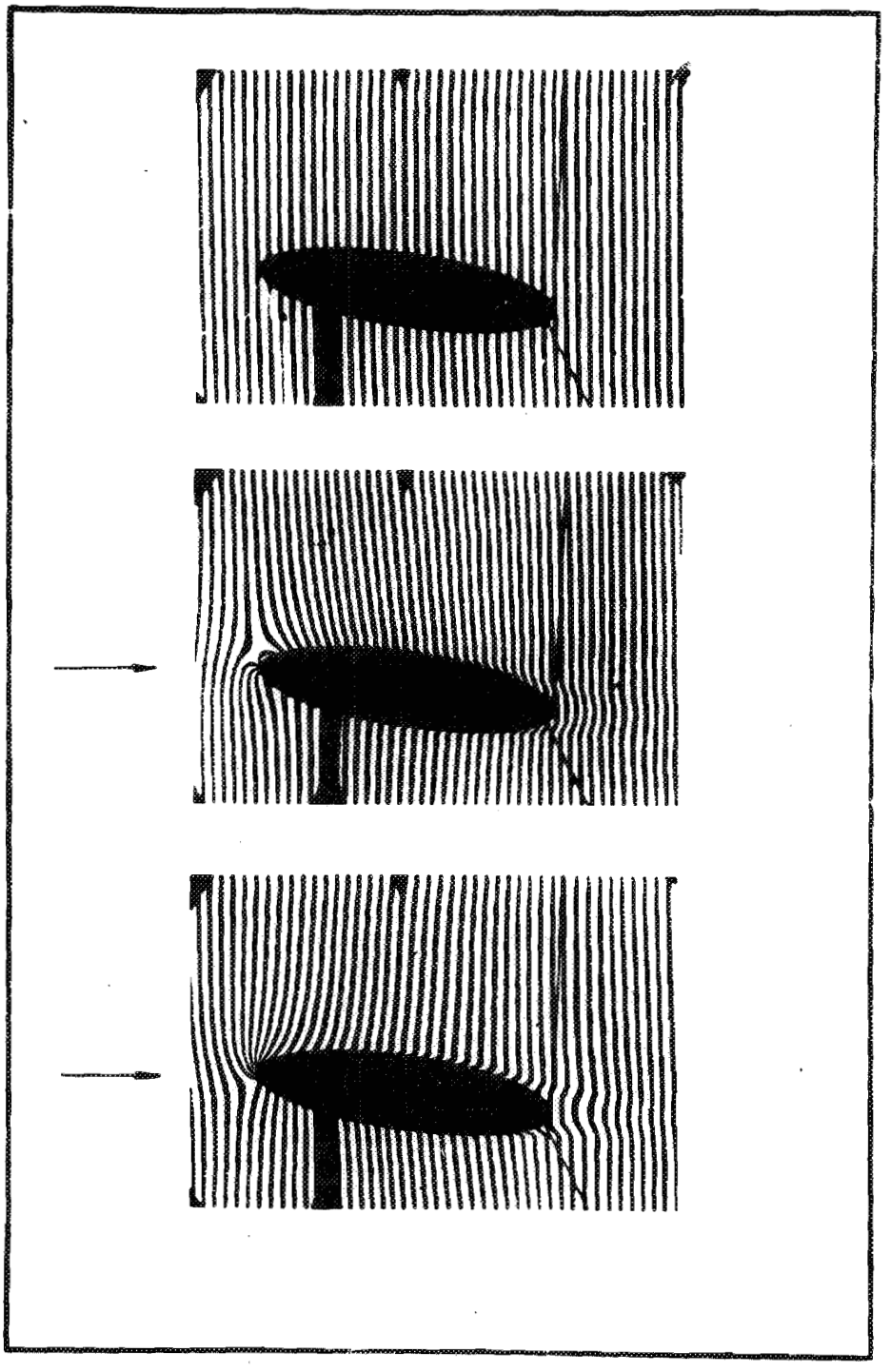

Fig. 10. Density Field on Elliptic Cylinder at $\alpha = 8^{\circ}$
$2a = 80$ mm; $\frac{b}{a} = \frac{1}{4}$; $L = 170$ mm; $v = 75$ m/sec.

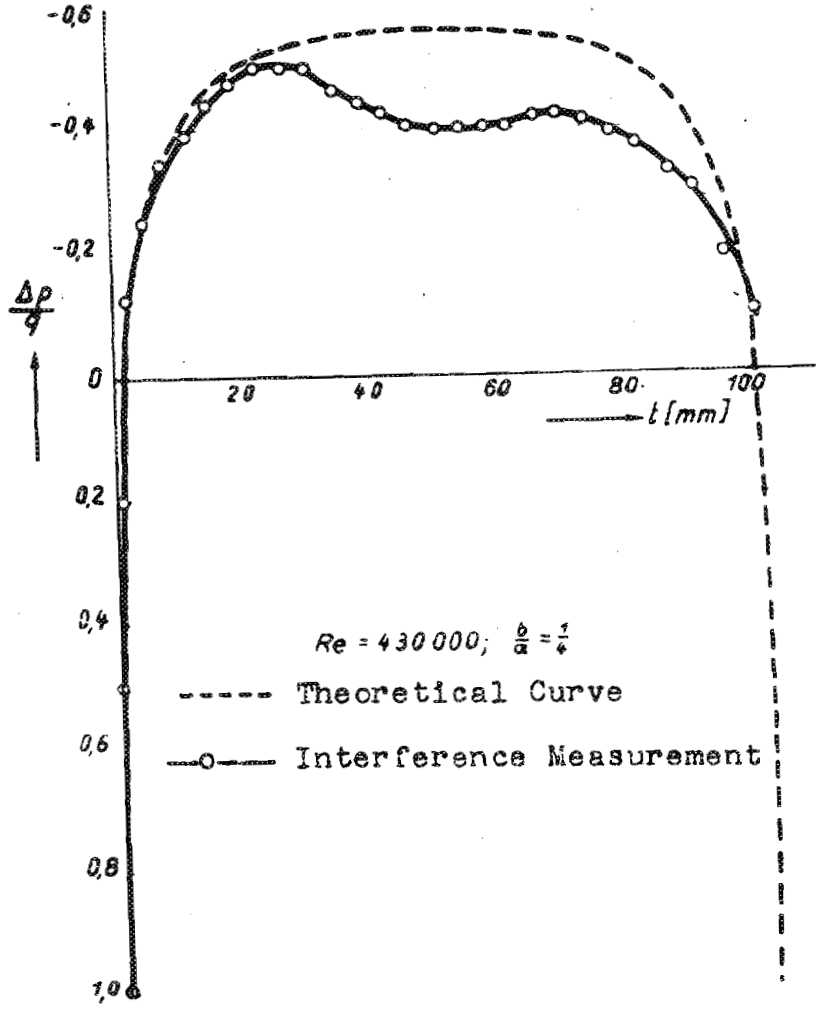

Fig. 11. Density Distribution on Elliptic Cylinder

$\alpha = 0°$

Fig. 12
Tech. Trans. TT-20

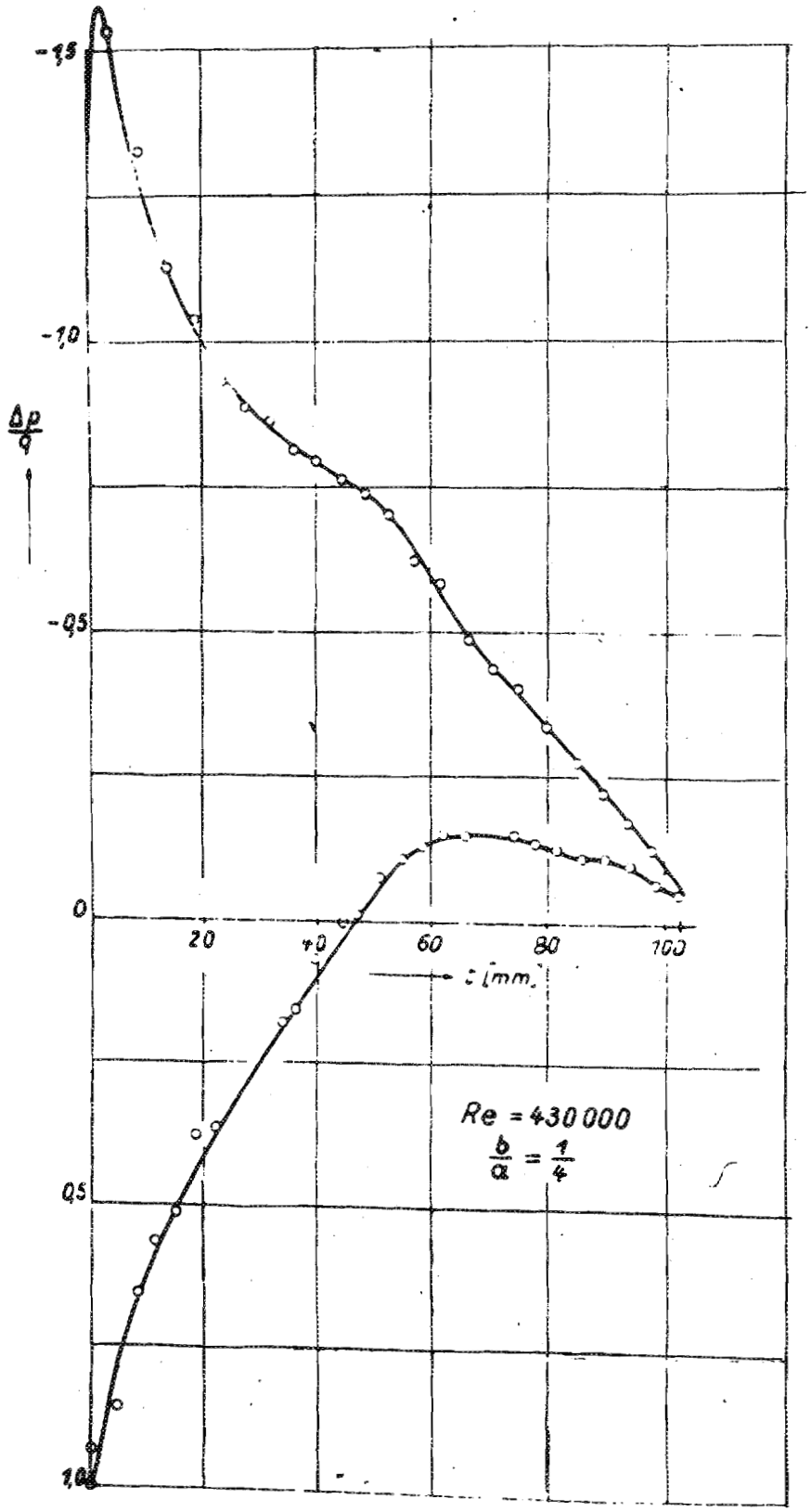

Fig. 12. Density Distribution on Elliptic Cylinder

$\alpha = 8°$

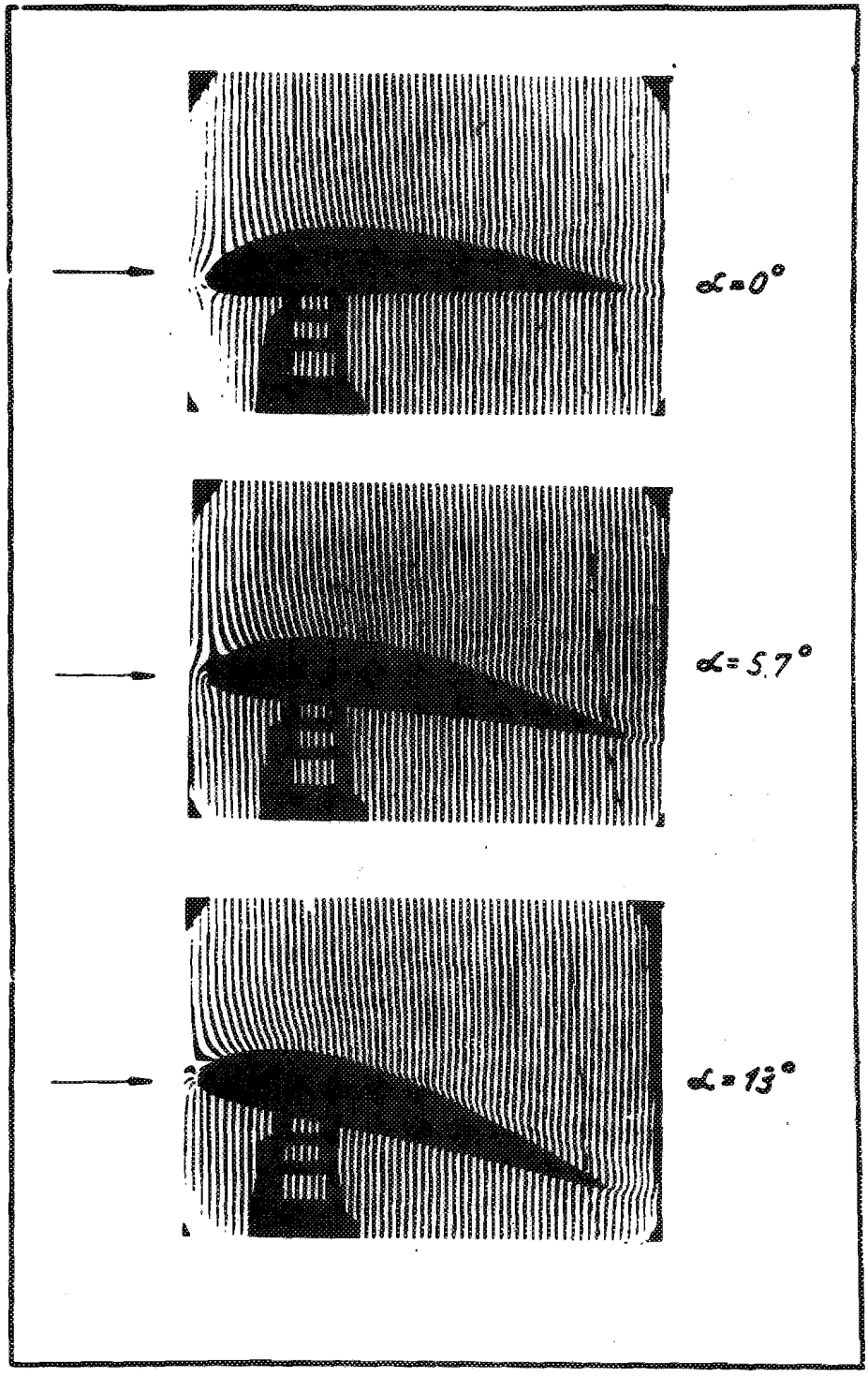

Fig. 13. Density Field on Profile Goettingen 387
Chord t = 120 mm.; Span L = 170mm.; v = 75 m/ sec.

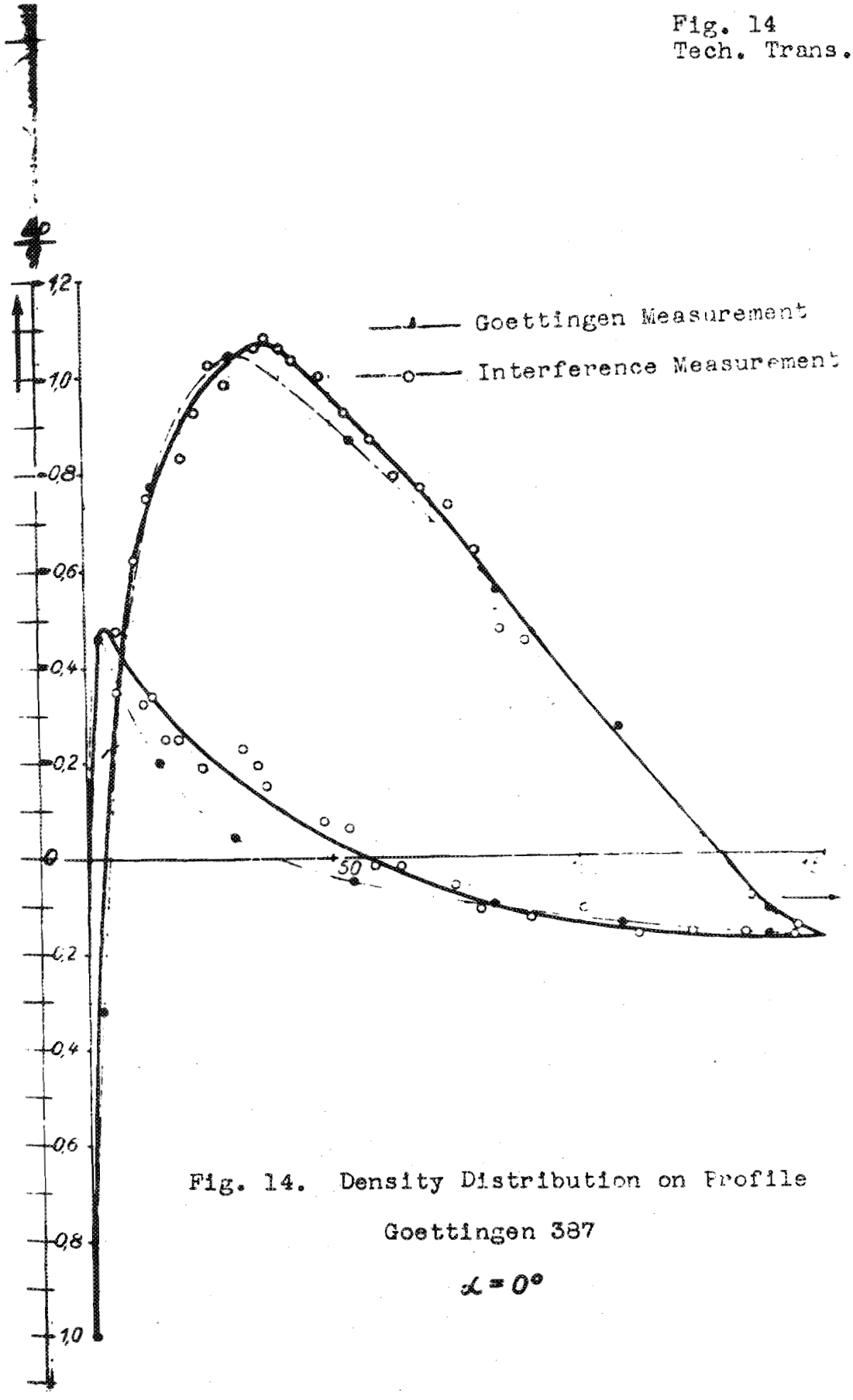

Fig. 14. Density Distribution on Profile

Goettingen 387

$\alpha = 0°$

---- Goettingen Measurement
—o— Interference Measurement

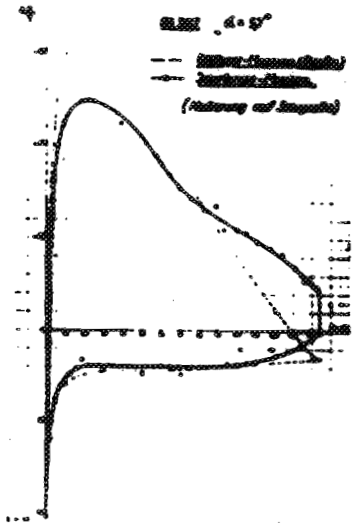

Fig. 15. Support on Suction Side

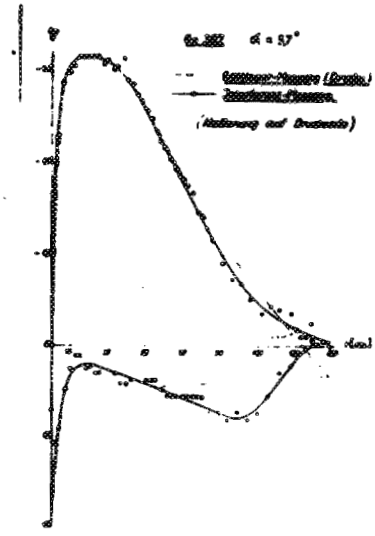

Fig. 16. Support on Pressure Side

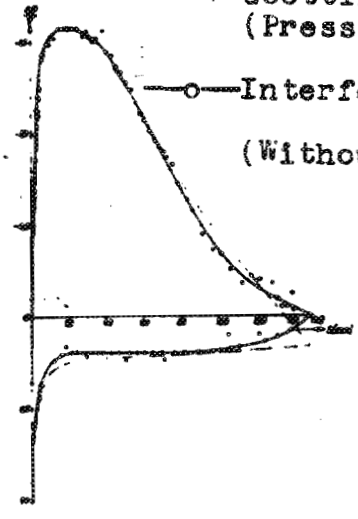

Fig. 17. Without Support

Influence of Support on Pressure Distribution

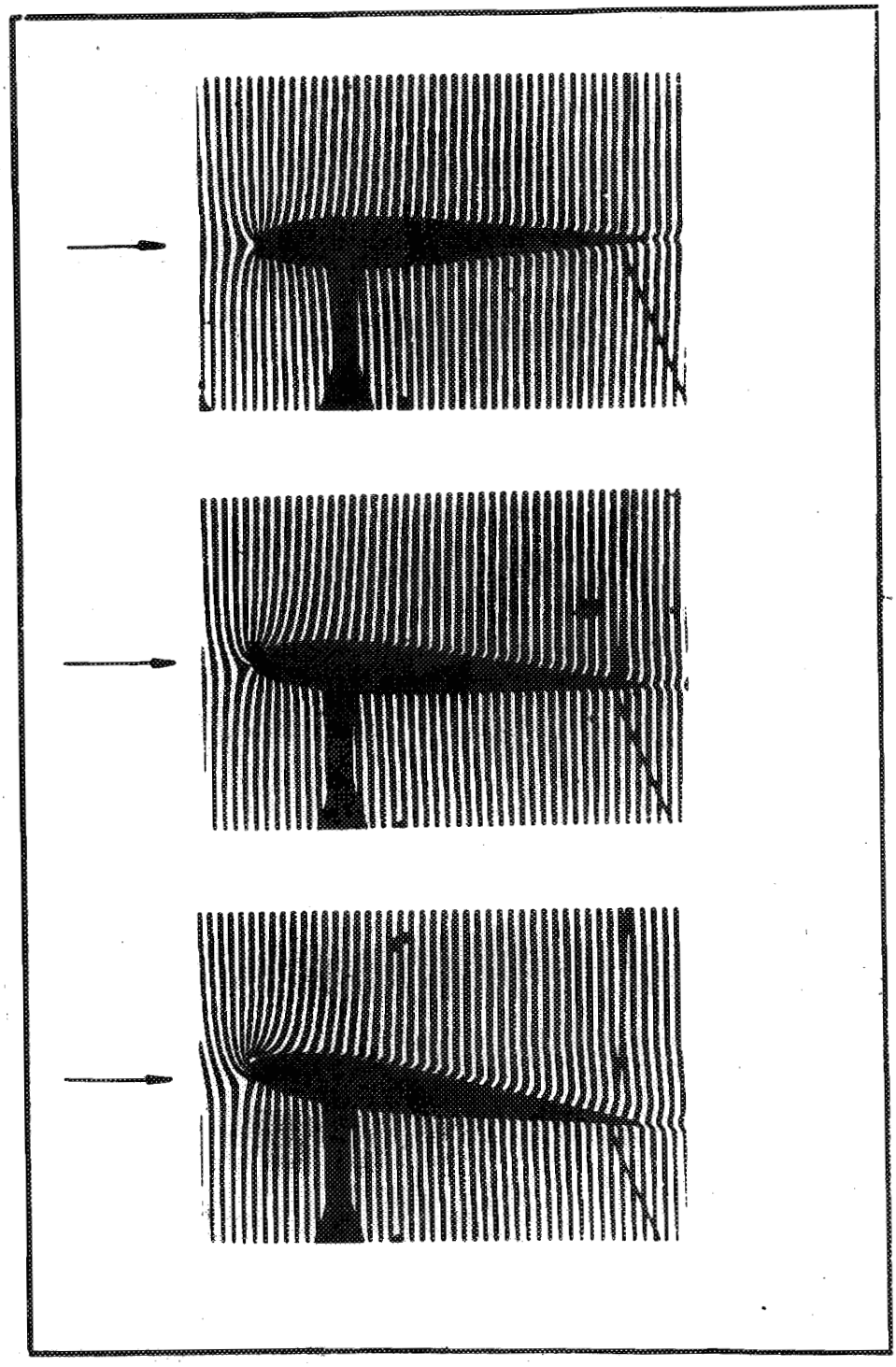

Fig. 18. Density Field on Symmetrical Joukowski Profile.
Chord t = 90 mm.; Span L = 170 mm.; v = 75 m/sec.

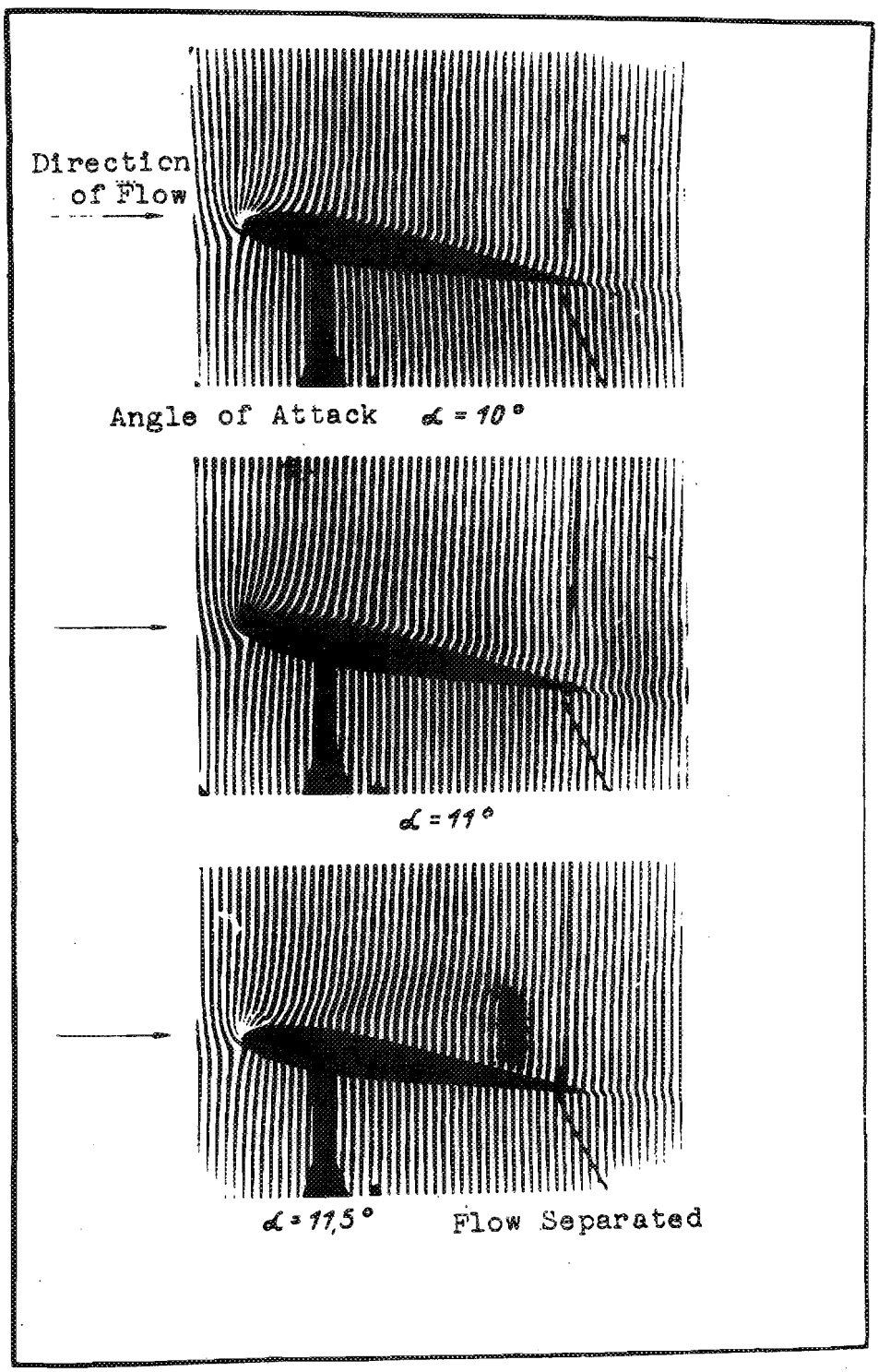

Fig. 19. Density Field on Symmetrical Joukowski Profile
Chord t = 90 mm.; Span L = 170 mm.; v = 75 m/sec.

Fig. 20

Zero-Interference
in Unfiltered Mercury Vapour Light

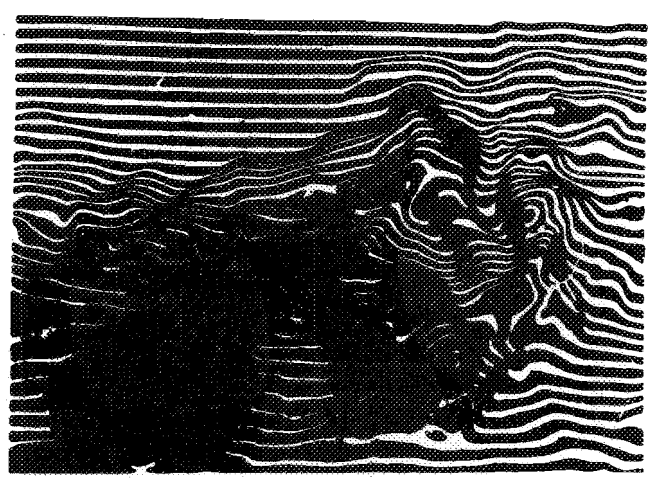

Fig. 26.
Non-steady Density Field around a Flame
Exposure time, 1/1000 sec.

Fig. 21
Tech. Trans. TT-20

-----Symmetrical Joukowski Profile from R-M 1315 [$\frac{d}{t}$=15%]
$\alpha = 0°$ $Re = 1{,}87 \cdot 10^6$

—o—Interference Measurement [$\frac{d}{t}$=12%] $Re = 48 \cdot 10^5$

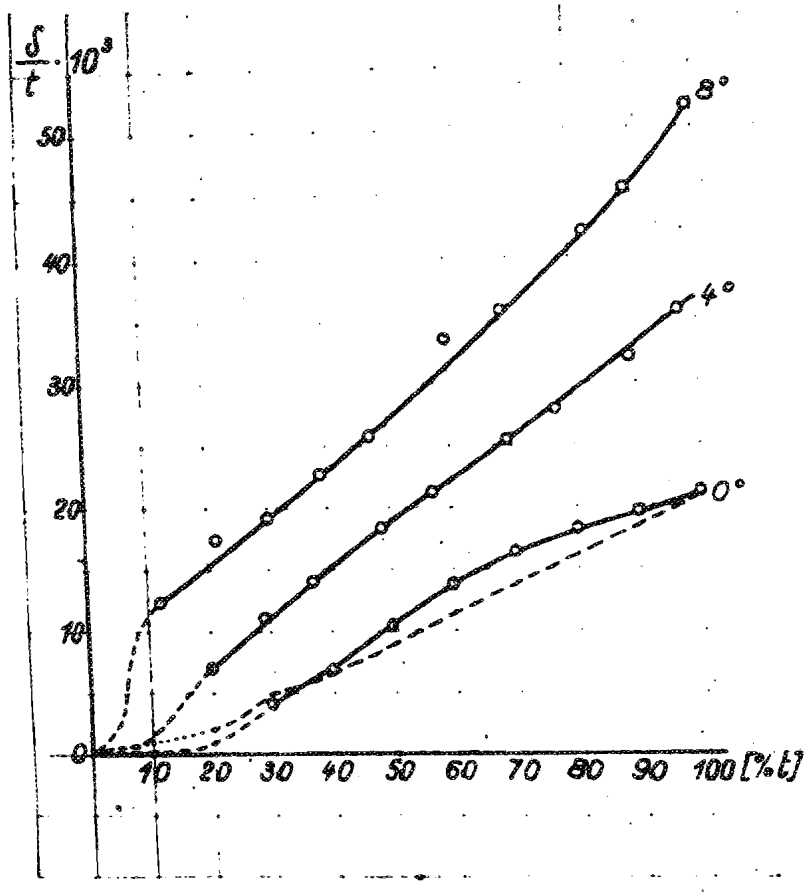

Fig. 21. Boundary Layer Thickness on Joukowski Profile

$\alpha = 0°; 4°; 8°$

Fig. 22
Tech. Trans. TT-20

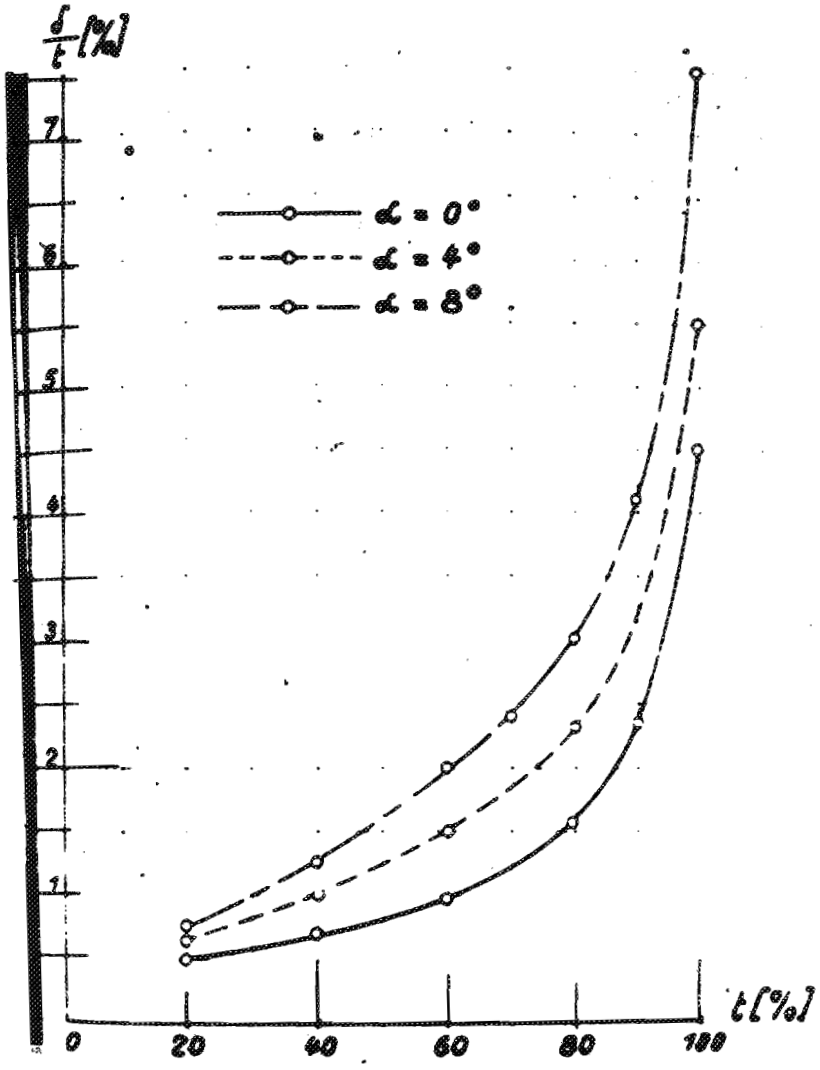

Boundary Layer Thickness on Elliptic Cylinder

v = 75 m/sec. b/a = 1/4 2a = 80 mm.

Fig. 22.

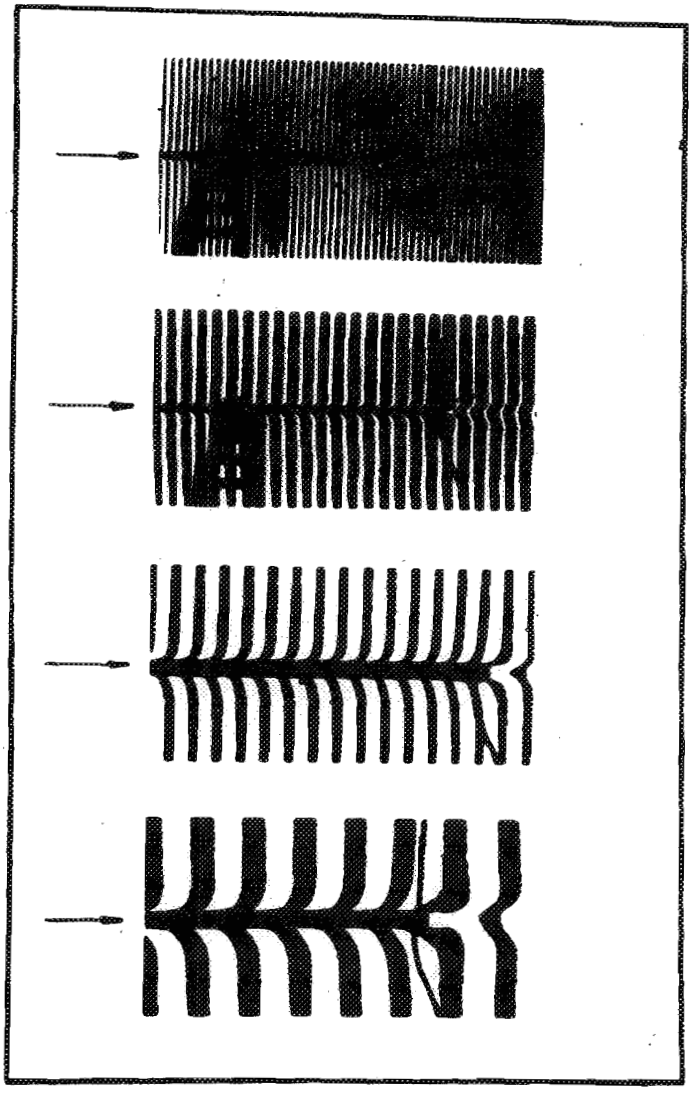

Fig. 23. Formation of Boundary Layer on a Flat Plate

Velocity Distribution in Boundary Layer
of Flat Plate

v = 75 m/sec.; t = 0.14 m

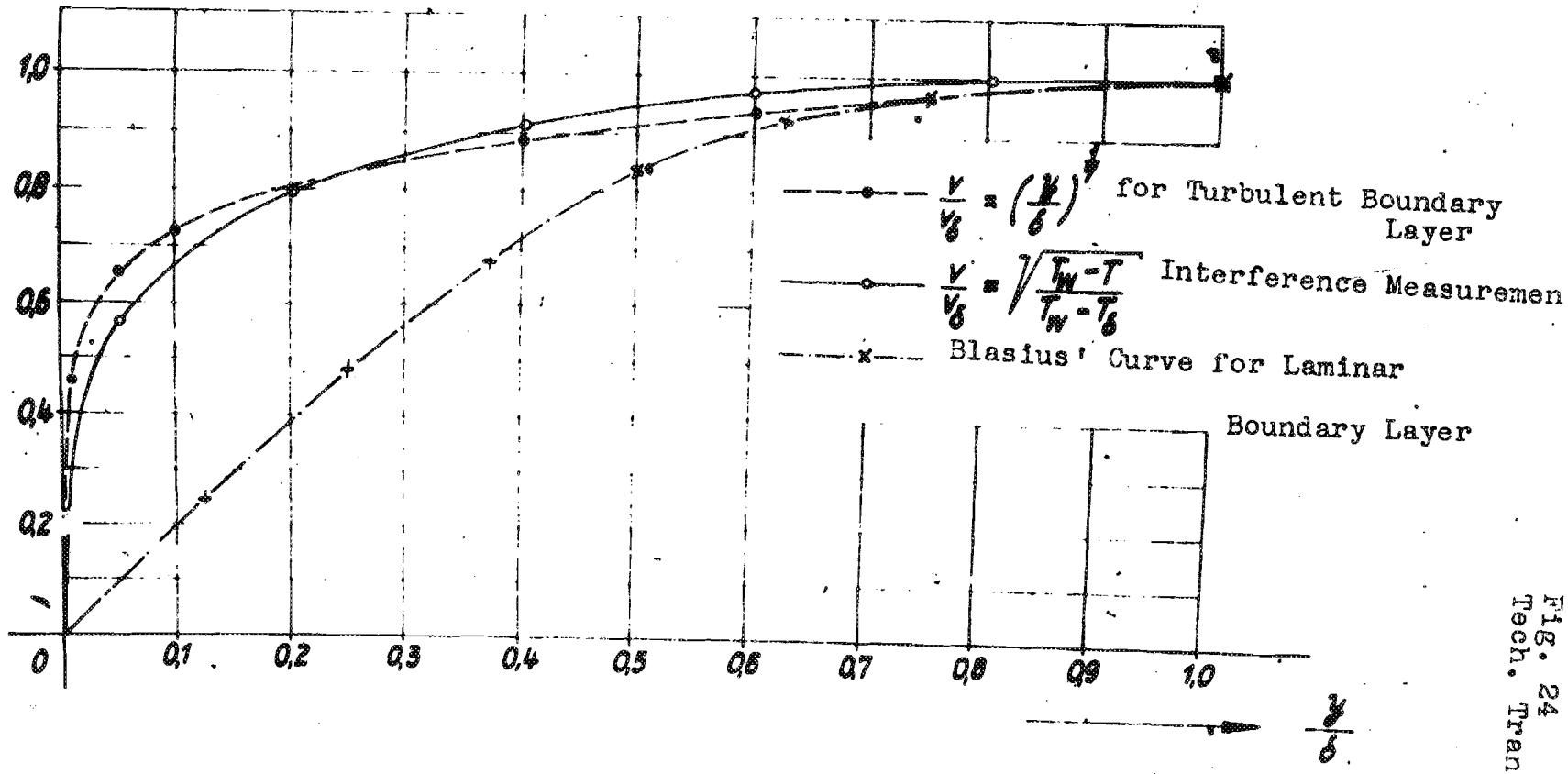

Fig. 24.

Fig. 24
Tech. Trans. TT-20

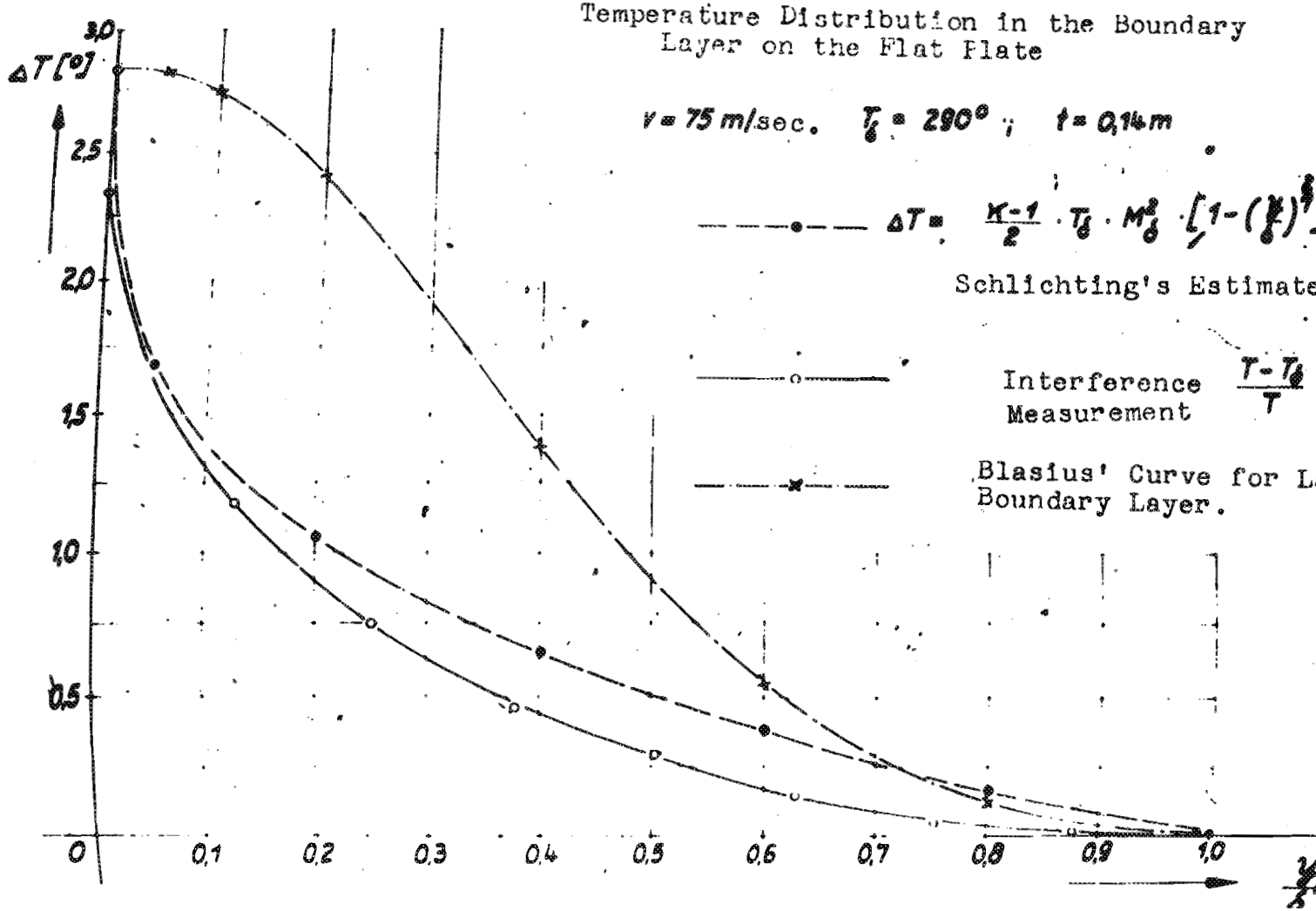

Fig. 25
Tech. Trans. TT-20

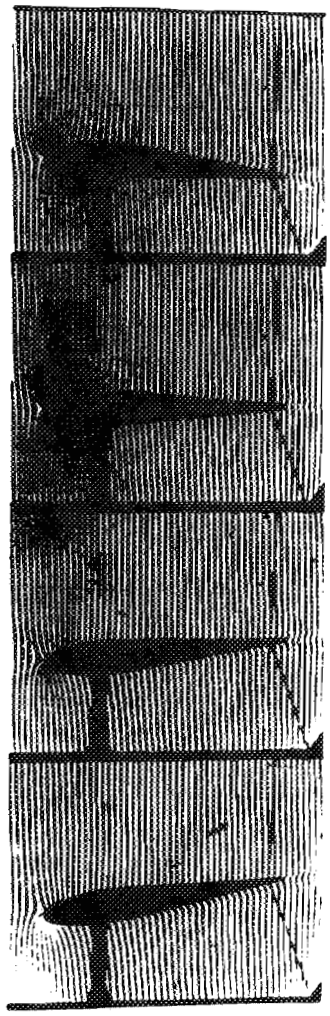

(a) Original Photograph

Fig. 27. Oscillating Joukowski Airfoil in Air Flow
n = 40 c.p.s.; v = 75 m/sec.

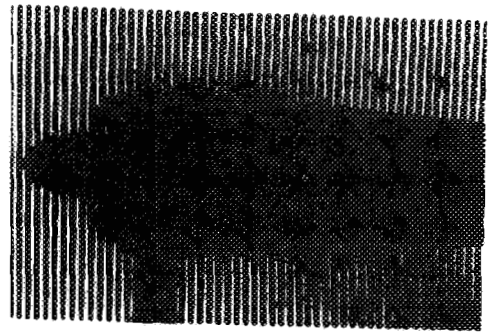

a

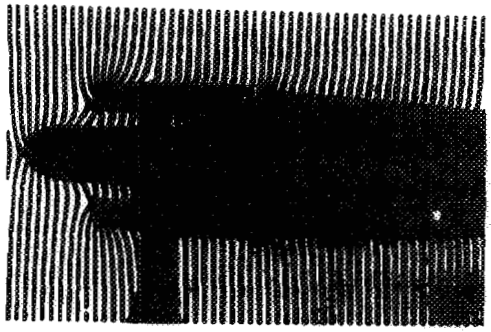

b

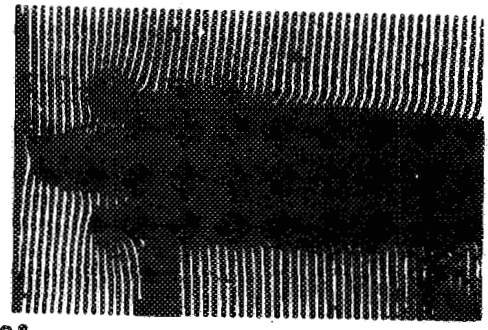

$\alpha = 0°$

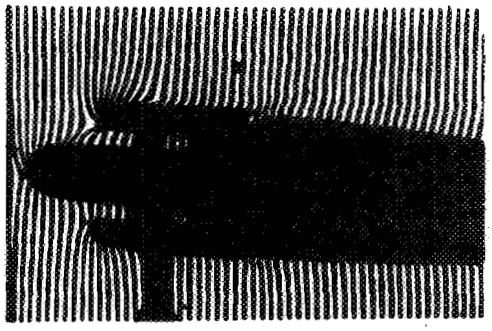

c

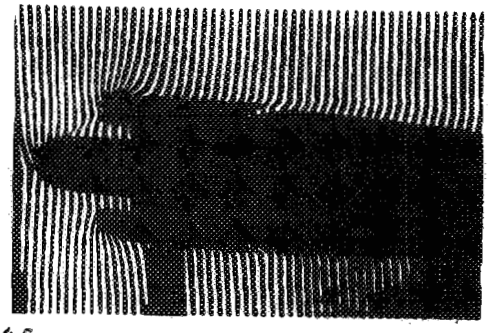

$\alpha = 4°$.

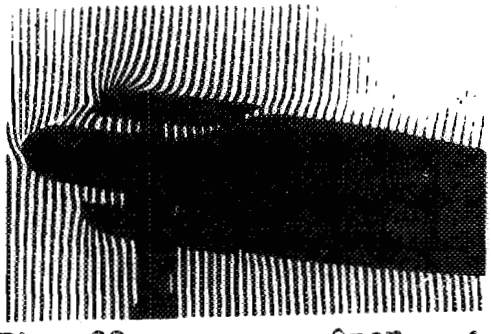

d

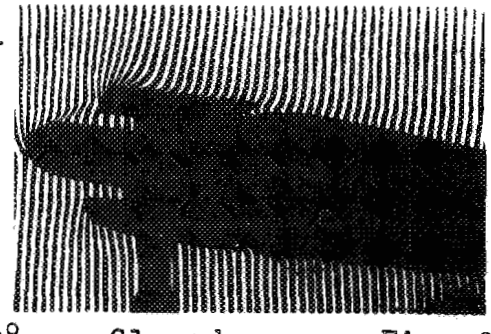

Fig. 28 — Open — $\alpha = 8°$ — Closed — Fig. 29

Flow Passage

Interference Field of the Flow around NACA Radiator Cowling with long Hub

v = 75 m/sec.

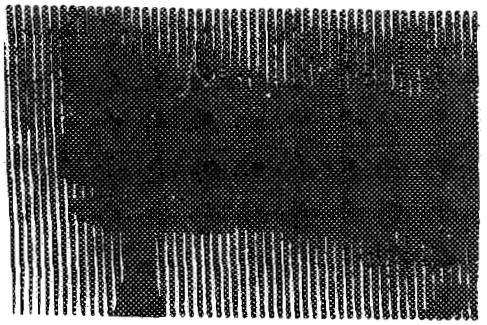

a

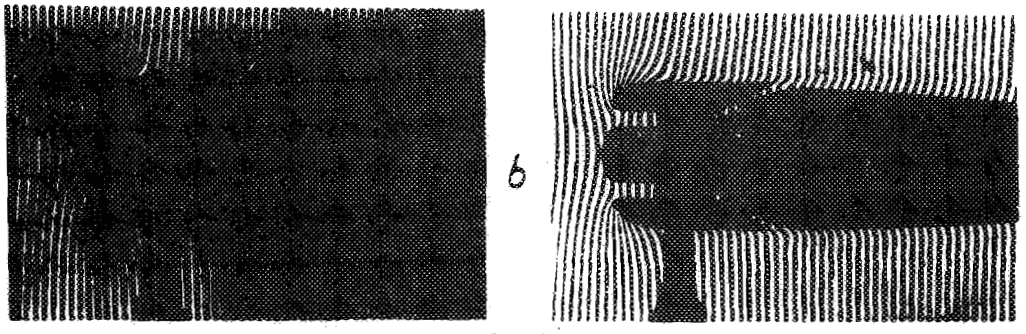

b

$\alpha = 0°$

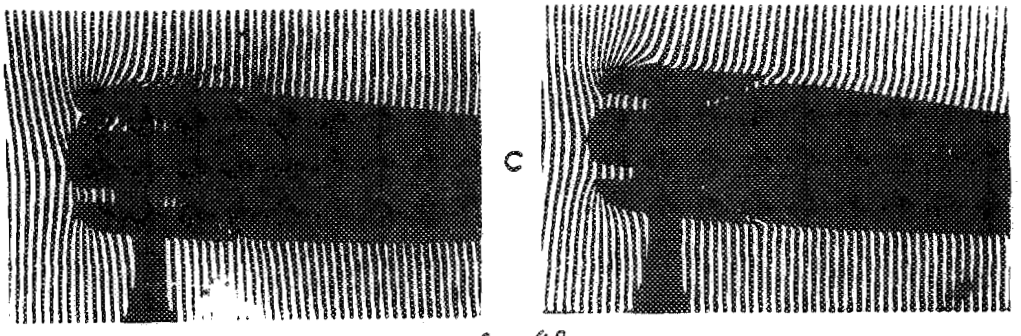

c

$\alpha = 4°$

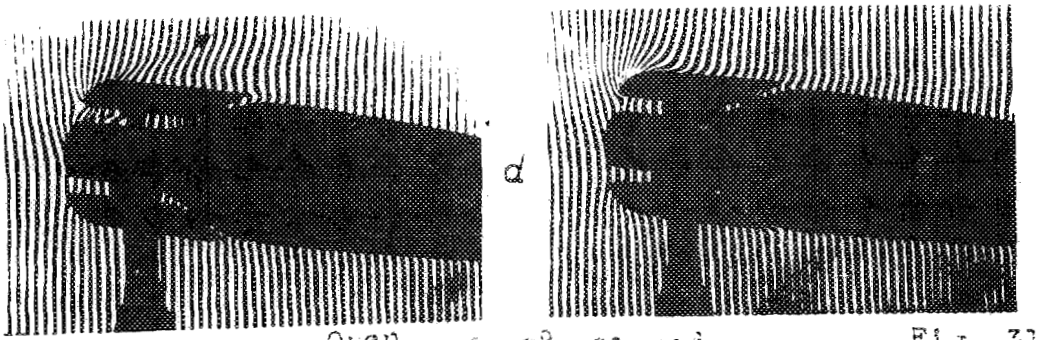

d

Fig. 30 — Open — $\alpha = 8°$ — Closed — Fig. 31

Flow Passage

Interference Field of the Flow around NACA Radiator Cowling with long Hub

v = 75 m/sec.

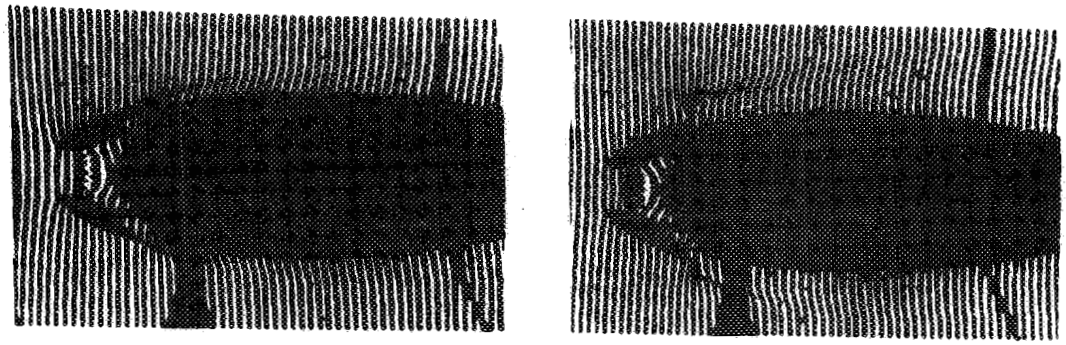

$\alpha = 0^\circ$

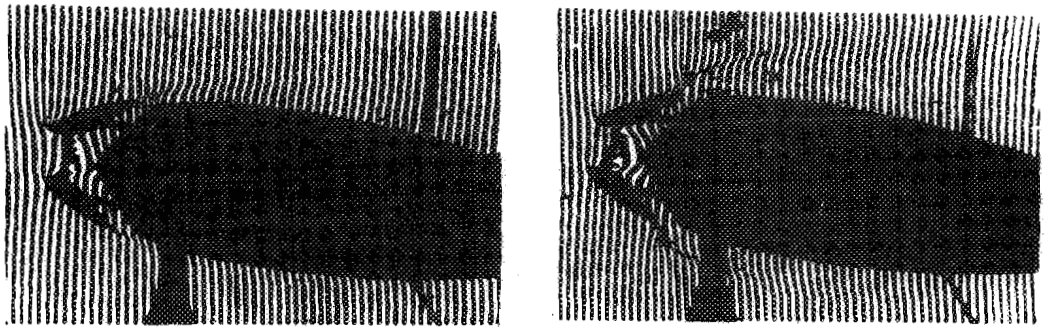

Fig. 32. $\alpha = 8^\circ$ Fig. 33.

Without — With
Hinged Flap

Radiator with Permeable Resistance Plate as Cooling Block

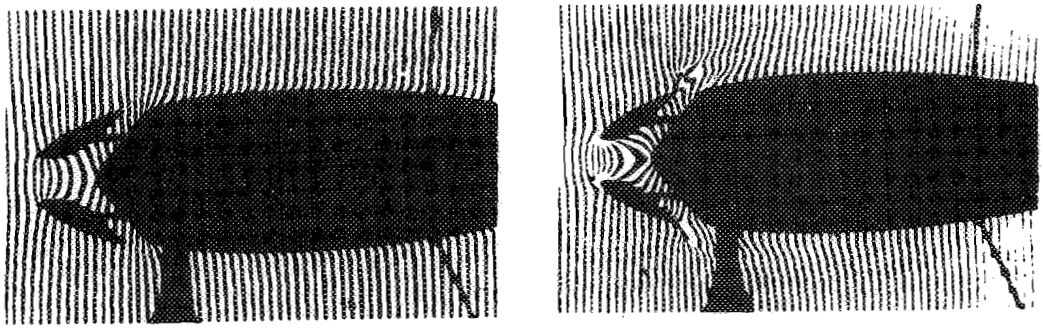

Fig. 34. $\alpha = 0^\circ$ Fig. 35.

Without — With
Hinged Flap
with Flow Passage Open

Interference Field of the Flow in a Nozzle Radiator with Very Wide Slit Opening

v = 75 m/sec.